Cell Reports

Article

Distinct types of intramitochondrial protein aggregates protect mitochondria against proteotoxic stress

Graphical abstract

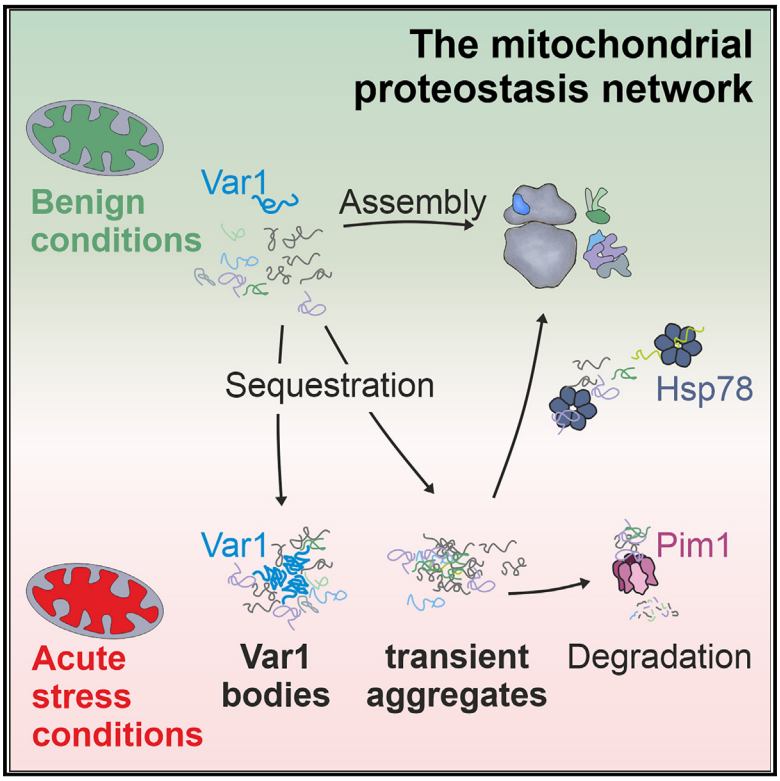

Authors

Lea Bertgen, Jan-Eric Bökenkamp, Tim Schneckmann, Christian Koch, Markus Räschle, Zuzana Storchová, Johannes M. Herrmann

Correspondence

hannes.herrmann@biologie.uni-kl.de

In brief

Bertgen et al. identify the mitochondria-encoded polyN protein Var1 as a nucleation factor for intramitochondrial protein aggregates. Var1 bodies form during acute stress to sequester misfolded matrix proteins. A distinct, more transient type of intramitochondrial aggregates is dissolved by the Hsp78 disaggregase and the Lon-related Pim1 protease.

Highlights

- Var1 bodies and Hsp78 foci represent distinct intramitochondrial aggregates
- Var1 bodies are formed from a mitochondria-encoded polyN protein
- Var1 bodies protect the mitochondrial proteome against acute stress
- The disaggregase Hsp78 and the Pim1 protease dissolve transient aggregates

Bertgen et al., 2024, Cell Reports *43*, 114018
April 23, 2024
https://doi.org/10.1016/j.celrep.2024.114018

CellPress

Cell Reports

CellPress
OPEN ACCESS

Article

Distinct types of intramitochondrial protein aggregates protect mitochondria against proteotoxic stress

Lea Bertgen,[1] Jan-Eric Bökenkamp,[2] Tim Schneckmann,[1] Christian Koch,[1] Markus Räschle,[2] Zuzana Storchová,[2] and Johannes M. Herrmann[1,3,*]

[1]Cell Biology, University of Kaiserslautern, RPTU, Erwin-Schrödinger-Strasse 13, 67663 Kaiserslautern, Germany
[2]Molecular Genetics, University of Kaiserslautern, RPTU, Paul-Ehrlich-Strasse 24, 67663 Kaiserslautern, Germany
[3]Lead contact
*Correspondence: hannes.herrmann@biologie.uni-kl.de
https://doi.org/10.1016/j.celrep.2024.114018

SUMMARY

Mitochondria consist of hundreds of proteins, most of which are inaccessible to the proteasomal quality control system of the cytosol. How cells stabilize the mitochondrial proteome during challenging conditions remains poorly understood. Here, we show that mitochondria form spatially defined protein aggregates as a stress-protecting mechanism. Two different types of intramitochondrial protein aggregates can be distinguished. The mitoribosomal protein Var1 (uS3m) undergoes a stress-induced transition from a soluble, chaperone-stabilized protein that is prevalent under benign conditions to an insoluble, aggregated form upon acute stress. The formation of Var1 bodies stabilizes mitochondrial proteostasis, presumably by sequestration of aggregation-prone proteins. The AAA chaperone Hsp78 is part of a second type of intramitochondrial aggregate that transiently sequesters proteins and promotes their folding or Pim1-mediated degradation. Thus, mitochondrial proteins actively control the formation of distinct types of intramitochondrial protein aggregates, which cooperate to stabilize the mitochondrial proteome during proteotoxic stress conditions.

INTRODUCTION

Protein homeostasis (proteostasis) is crucial for the function of cells and the health of organisms.[1] Stress conditions lead to an increase of the folding capacity of the chaperone network and an upregulation of the ubiquitin-proteasome system. When the folding and degradation systems are overstrained, a third layer of defense becomes important: nucleating factors promote the sequestration of misfolded proteins into aggregates.[2] Such nucleating factors are present in different cellular compartments where they bind specific sets of protein clients. Whereas some of these aggregates are benign and well tolerated, others are toxic. However, whether these aggregates themselves jeopardize proteostasis or whether their occurrence is the consequence of proteotoxic conditions is often not clear.

The baker's yeast *Saccharomyces cerevisiae* proved to serve as an excellent model system to unravel the biology of different types of aggregates.[3] The small heat shock protein Hsp42 functions as a nucleation factor that induces the formation of cytosolic small aggregates, termed cytoQs or Q bodies[4] (Figure 1A). These small foci coalesce upon prolonged stress conditions into larger structures that often associate with the surface of the nuclear envelope (juxtanuclear quality control aggregates).[3,5] Similar structures can also form in the nucleus (intranuclear quality control aggregates)[6] as well as in mitochondria. In mammalian cells, small heat shock proteins are also targeted into the intermembrane space of mitochondria where they induce the formation of aggregates that contain superoxide dismutase (Sod1) among other proteins.[7] Protein aggregates were also observed in the mitochondrial matrix, for example, upon inhibition of the matrix processing peptidase[8] or of mitochondrial chaperones,[9,10] or upon expression of folding-incompetent proteins.[11]

Accumulation of selected groups of proteins in the cytosol can induce more specialized cytosolic aggregates such as MitoStores, which sequester non-imported mitochondrial precursor proteins.[12,13] Hsp104, a hexameric machine in the cytosol and nucleus of yeast can promote the release of proteins from aggregates.[14–16]

Distinct from these rather benign aggregates are those that contain the pathogenic versions of human huntingtin.[17,18] Upon expression in yeast, this protein is sequestered by Rnq1, an endogenous polyglutamine (polyQ) protein of the yeast cytosol. Rnq1 nucleates the formation of insoluble protein deposits, which pose a severe threat to cellular function.

Mitochondria contain a tiny genome that codes for a small number of mostly hydrophobic membrane proteins. In fungi, plants, and many unicellular eukaryotes, but not in animals, the ribosomal subunit Var1 (uS3m) is also mitochondrially encoded.[19,20] Why the *VAR1* gene was retained in mitochondria is not clear, since it was shown that a nuclear-encoded fusion protein with a mitochondrial targeting signal (MTS) is functional.[21]

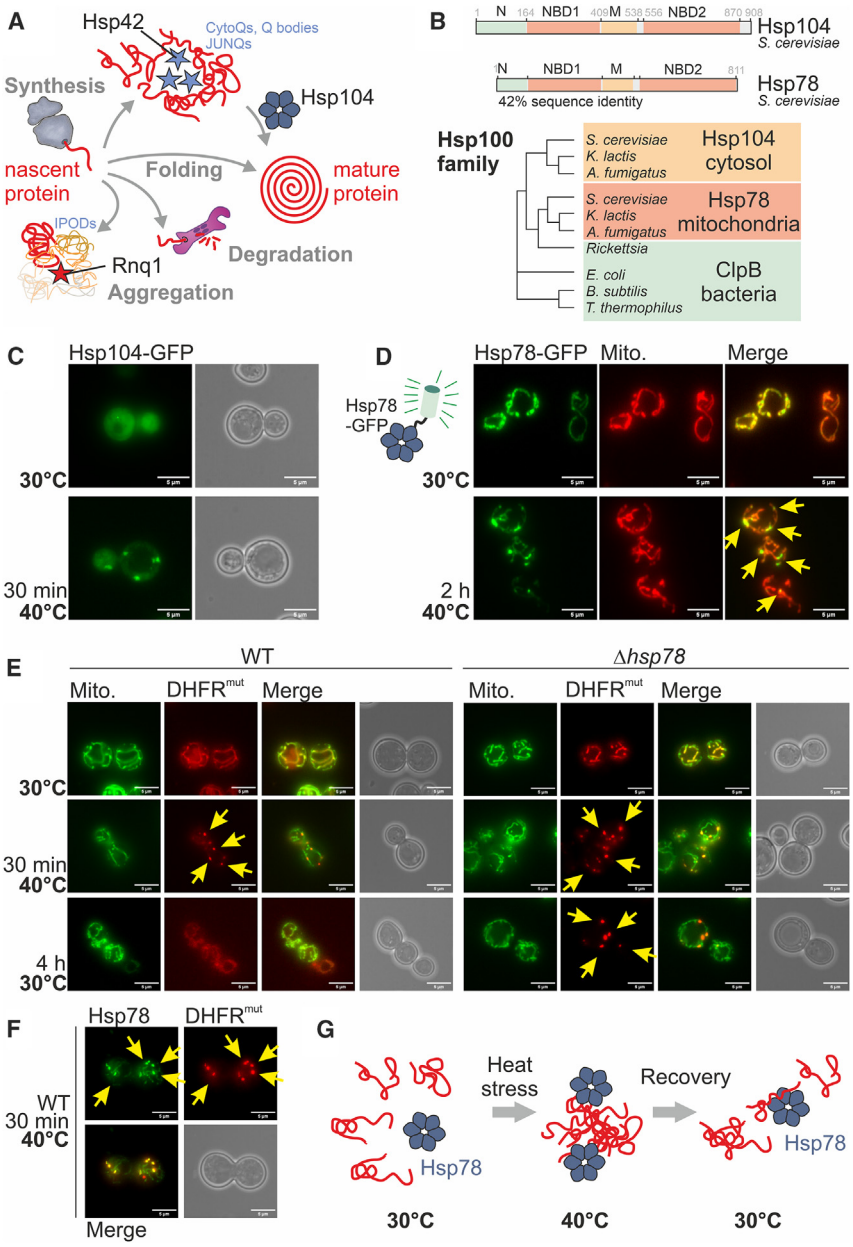

Figure 1. Hsp78 associates with mitochondrial aggregates

(A) Schematic representation of the proteostasis network of the yeast cytosol.

(B) Hsp104 and Hsp78 are structurally and phylogenetically related. NBD, nucleotide binding domain; M, middle domain.

(C) Hsp104-GFP was expressed in wild-type yeast cells grown on galactose medium at 30°C and shifted to 40°C for 30 min.

(D) Cells expressing Hsp78-GFP and mitochondria-targeted mScarlet (mt-mScarlet, Mito.) were grown in galactose medium at 30°C (top) and shifted for 2 h to 40°C (bottom). Arrowheads depict the Hsp78-bound aggregates.

(E and F) Cells expressing mitochondria-targeted GFP (mtGFP, Mito.) or Hsp78-GFP and DHFR^{mut}-mScarlet under control of a *GAL* promoter were grown on raffinose medium to log phase at 30°C and induced by addition of galactose. Cells were shifted to 40°C for 30 min before they were allowed to recover at 30°C for 4 h. Arrows show DHFR^{mut}-containing aggregates.

(G) Scheme of Hsp78-mediated disaggregation.

Most mitochondrial proteins are synthesized in the cytosol and imported into mitochondria.[22] In the matrix, these proteins are folded by the mitochondrial chaperone system or, if folding fails, degraded by the hexameric protease Pim1, a homolog of the bacterial Lon protease.[23,24]

In this study, we explored the formation of protein aggregates in the matrix. We identified two distinct types of aggregates: first, we observed that Hsp78 binds transiently to dynamic intramitochondrial granules, which largely consist of nuclear-encoded proteins; second, we identified a second, more persistent aggregate type that is nucleated by non-assembled Var1. These Var1 bodies sequester misfolded proteins and stabilize the mitochondrial proteome under acute stress conditions. Thus, yeast mitochondria employ nuclear and mitochondrially encoded factors that control the sequestration of potentially harmful proteins by the formation of distinct types of protein aggregates.

RESULTS

The AAA protein Hsp78 associates with mitochondrial aggregates

The yeast cytosolic chaperone Hsp104 and the bacterial ClpB are well-characterized AAA chaperones that resolve protein aggregates.[14,25,26] The Hsp78 protein of the mitochondrial matrix is closely related to these proteins and shares the same architecture (Figures 1B, S1, and S2A). GFP fusions to Hsp104[27] proved to serve as excellent markers for the visualization of cytosolic protein aggregates (Figure 1C). Following the same strategy, we expressed Hsp78 fused to GFP in wild-type cells, which was well tolerated, did not affect cellular growth (Figure S2B), and was largely inaccessible to added protease verifying its intramitochondrial location (Figure S2C). In cells grown under non-stressed conditions, Hsp78-GFP was distributed throughout the mitochondrial network (Figure 1D). However, upon exposure of cells to acute heat stress conditions (40°C for 2 h), Hsp78-GFP formed punctate structures within mitochondria, indicating its association with intramitochondrial aggregates (Figure 1D, arrows) and confirming previous observations.[10,28,29] Heat stress conditions induced Hsp78 aggregation also in cells in which translation had been blocked in the cytosol or in mitochondria, as well as in *rho*^{0} cells lacking mitochondrial DNA (Figures S2D–S2F).

Thus, Hsp78 showed a very robust aggregation behavior that was independent of newly synthesized proteins.

To study the role of Hsp78 for mitochondrial proteostasis, we used a mitochondria-targeted version of $DHFR^{mut}$ as a model protein. This well-established model consists of a mitochondrial presequence followed by a folding-incompetent variant of mouse dihydrofolate reductase carrying three point mutations (C7S, S42C, N49C).[30] In wild-type cells, $DHFR^{mut}$ aggregated upon exposure to high temperature (40°C) but became again dispersed once cells were shifted back to non-stress conditions (4 h at 30°C, Figure 1E). In contrast, in *Δhsp78* cells, $DHFR^{mut}$-containing aggregates were not resolved, indicating that Hsp78 disentangles these intramitochondrial aggregates and promotes the recovery of the mitochondrial proteome (Figure 1E). During the stress conditions, Hsp78 and $DHFR^{mut}$ co-localized in the same aggregates (Figure 1F).

We also tested the effect of another misfolded protein: expression of the folding-incompetent G255R mutant of carboxypeptidase Y (CPY*)[31] in mitochondria, which had a strong effect on cellular growth at normal and increased temperatures (Figures S3A–S3C) and was correctly targeted into mitochondria (Figure S3D), but neither interfered with the ability of mitochondria to synthesize mitochondrial translation products (Figure S3E) nor with the import competence of mitochondria per se (Figures S3F–S3H). The matrix-targeted mtCPY* formed aggregates also at non-heat conditions, which permanently co-localized with Hsp78; apparently, Hsp78 was not able to resolve the aggregates formed by this folding-incompetent protein (Figures S4A–S4H). We conclude that Hsp78 interacts with intramitochondrial aggregates and facilitates their dissociation once stress conditions are overcome (Figure 1G).

Hsp78 prevents the Pim1-mediated degradation of mitochondrial proteins

To identify endogenous interaction partners of Hsp78, we isolated Hsp78-GFP from wild-type and rho^0 yeast cells by Sepharose-coupled nanobodies and analyzed the bound proteins by mass spectrometry (Figures 2A and S5A–S5G). Many mitochondrial proteins were co-purified with Hsp78 including many subunits of the mitochondrial ribosome (Figures 2B, S5D, and S5E; Table S1). In rho^0 cells, which lack a mitochondrial genome and therefore do not express mitochondrial rRNAs, mitoribosomal proteins cannot assemble and were considerably enriched on Hsp78 (Figures 2B and 2C; Table S1). This observation supports recent studies that have proposed a function of Hsp78 as a binding partner of newly imported but not yet folded and assembled mitochondrial proteins.[10,28]

Mutants lacking Hsp78 do not show a reduced growth rate under respiratory conditions; however, they need longer to recover from the exposure to heat shock (Figures 2D and S6A). To study the relevance of Hsp78 for the aggregation behavior of an endogenous mitochondrial protein, we chose Aim17 because of its aggregation-prone nature.[12] We expressed a mCherry-tagged version of Aim17 (Figure S6B) that showed a dispersed mitochondrial distribution at 30°C (Figure S6C). Upon exposure to 40°C for 30 min, however, Aim17 formed intra-mitochondrial aggregates that co-localized with Hsp78-GFP (Figure 2E). The aggregation of Aim17 was still seen when cells had been pretreated with cycloheximide for 2 h, suggesting that aggregation is not restricted to newly synthesized Aim17 (Figures S6D and S6E). When we shifted the temperature back to 30°C, the aggregation of Aim17 was reversible within wild-type mitochondria after the heat shock; interestingly, the dissociation of Aim17 was retarded in *Δhsp78* cells, suggesting that Hsp78 can promote its disaggregation (Figures 2F–2H). This suggests that Hsp78 does not prevent protein aggregation per se but facilitates the dissociation of aggregates.

This inspired us to look for a potential functional interaction of Hsp78 with Pim1.[42] It has been reported before that *in vitro*, overexpressed Hsp78 protects newly imported model proteins from Pim1-mediated degradation.[43] The substrate spectrum of members of the Lon protease family was previously analyzed by co-isolation with catalytically inactive mutants.[44] Following the same approach, we generated an S1015A point mutant of Pim1 (Figure S7A), which destroys the essential serine-lysine dyad of its active site.[45,46] We made use of a *Δpim1* suppressor strain that maintains its mitochondrial genome[42] and expressed either Pim1 or the non-functional mutant, both with C-terminal HA tags. The $Pim1^{S1015A}$ mutant did not complement the growth defect of the deletion strain (Figures S7B and S7C). Nevertheless, the mutated Pim1 protein accumulated in mitochondria (Figure S7D) and was even converted over time to the matured protein species as verified by import experiments with radiolabeled $Pim1^{S1015A}$ protein (Figure S7E).

We expressed $Pim1^{S1015A}$ as an HA-tagged version in wild-type and *Δhsp78* cells, purified the protein from Triton X-100-lysed cell extracts (Figure S7F), and performed mass spectrometry of the bound fractions (Figures 2I and S7G). Pim1 was efficiently purified from both wild-type and Δ*hsp78* cells (Figure 2J; Table S1). In addition, established interactors of Pim1 such as Mam33, Mrx6, and Pet20 were co-purified (Figure 2J; Table S1). In extracts of *Δhsp78* cells, more mitochondrial proteins co-eluted with Pim1, indicating that the absence of Hsp78 leads to the increased Pim1-mediated degradation of mitochondrial proteins (Figure 2K; Table S1).

In summary, our observations suggest that Hsp78 protects proteins against Pim1-mediated degradation in mitochondria, consistent with previous observations.[43] The underlying mechanisms must be analyzed in the future, but it appears likely that Hsp78 and Pim1 compete for the same misfolded substrates (Figure 2L) to either convert them into their native folded conformation (Hsp78), or to degrade them (Pim1).

Mitochondrial protein synthesis protects against intramitochondrial stress

Although many nuclear-encoded mitochondrial proteins are apparently substrates of Hsp78, we did not find mitochondrial translation products in the Hsp78 interactome. We therefore tested whether mitochondrial translation products are relevant for the resistance of cells against acute heat stress. To this end, we grew wild-type cells for 16 h with or without chloramphenicol, which inhibits mitochondrial protein synthesis, but not cytosolic translation. Subsequently, we subjected the cells to a short acute heat shock at 45°C or 50°C for 5 min and then counted surviving cells after plating on glucose medium

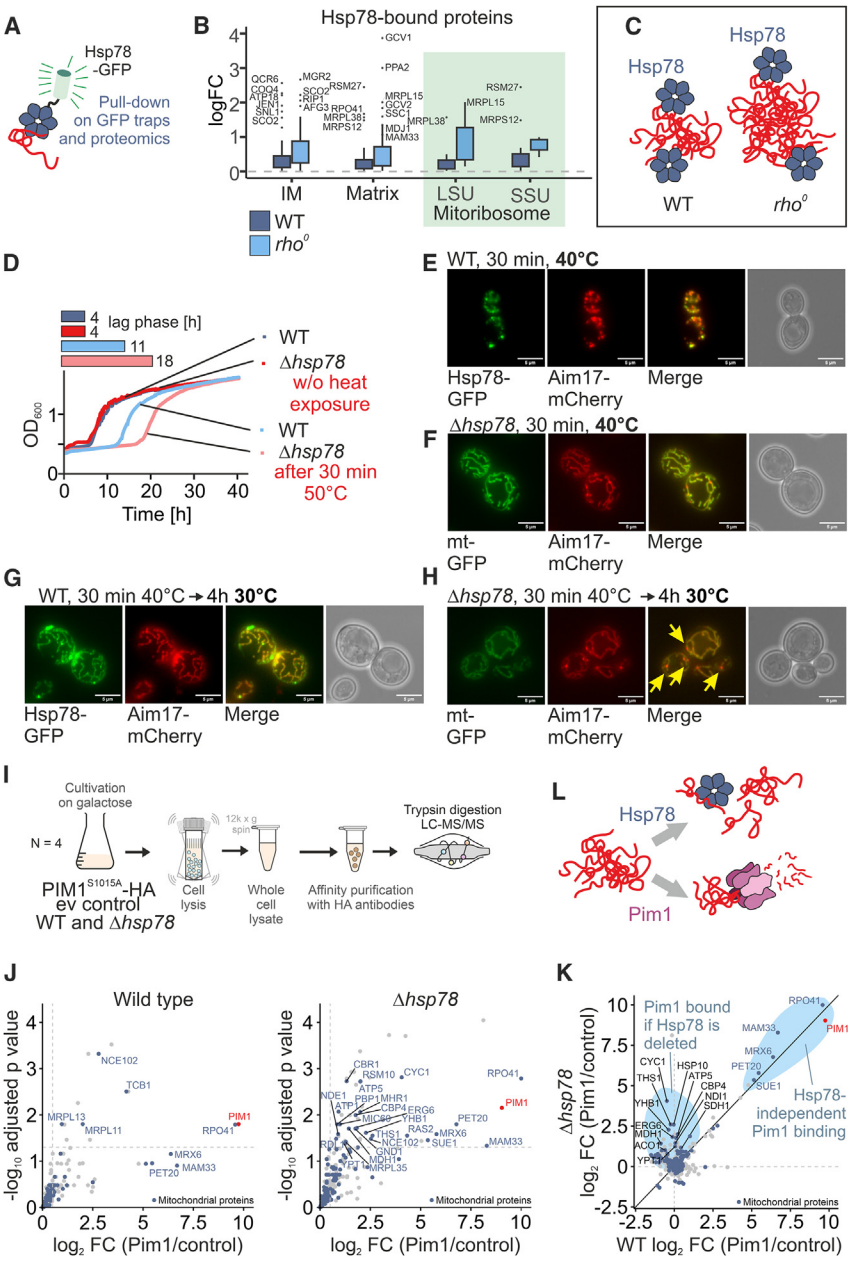

Figure 2. Hsp78 helps cells to recover from acute heat stress

(A–C) Hsp78-GFP or mtGFP for control were expressed in wild-type and *rho*^{0} cells on galactose medium at 30°C. Cells were lysed and extracts were subjected to affinity purification on GFP-binding nanobodies. The eluates were analyzed by mass spectrometry. The relative enrichment (log2 fold change, log FC) of proteins in the Hsp78-GFP vs. GFP is shown for specific groups of proteins. See STAR methods for information about the experimental details.[32–41]

(D) Cells grown at 30°C were exposed to 50°C or 30°C for 30 min before their growth at 30°C was continuously measured for 2 days.

(E–H) Wild-type or *Δhsp78* cells expressing mtGFP or Hsp78-GFP were grown to log phase in raffinose medium at 30°C. Then, by addition of 0.5% galactose the expression of Aim17-mCherry was induced for 4 h. The expression was stopped and cells were shifted to a heat shock at 40°C for 30 min. For recovery, cells were shifted back to 30°C. Aim17 still remained aggregated in *Δhsp78* cells after the recovery phase (arrowheads).

(I and J) Proteomics of the proteins co-isolated with Pim1^{S1015A}-HA from extracts of wild-type and *Δhsp78* cells. Plotted are proteins that are of increased abundance in the Pim1-containing samples in comparison with the empty vector control. Mitochondrial proteins are shown in blue. Names of the subunits of the Pim1-Mrx6-Mam33-Pet20 complex are indicated.

(K) Correlation plot comparing the enrichment factors (log2 fold changes) of the Pim1 interactors from wild-type and Δ*hsp78* cells.

(L) The observation that Δ*hsp78* cells increase the substrate binding to Pim1 suggests that Pim1 and Hsp78 compete for the same client proteins.

(Figures 3A and 3B). Surprisingly, we found that chloramphenicol pretreatment strongly impaired the resistance against heat stress, and almost all pretreated cells were killed by exposure to 50°C, even though this short exposure was tolerated well by non-pretreated cells. Thus, mitochondrial translation products directly or indirectly protect cells against acute heat stress.

We wondered which of the eight mitochondrially encoded proteins was relevant for the stress resistance. The mitochondrial genome encodes for seven core subunits of respiratory chain enzymes and, in addition, for one ribosomal protein, Var1 (Figure 3C). Since we found a similar heat sensitivity in respiratory deficient mutants and wild-type cells, we reasoned that respiration per se is not critical for heat stress resistance. To elucidate the role of Var1 independently of mitochondrial translation, we made use of MTS-Var1, a nuclear-encoded version of Var1 (Figure 3D). MTS-Var1 consists of the MTS of Cox4 fused to a Var1 sequence that was adapted to the universal genetic code (rather than the mitochondria-specific code).[21] Upon expression in cells that lack the *VAR1* gene in their mitochondrial DNA, MTS-Var1 was targeted to mitochondria, partially rescuing the respiration deficiency of *VAR1* mutants (Figure 3D) and restoring their ability to synthesize mitochondrially encoded proteins (Figure 3E). However, we also noticed that MTS-Var1 expression reduced the fitness of non-respiring cells, indicating a translation-independent negative effect of this fusion protein (Figure 3D).

The nuclear-encoded MTS-Var1 protein allowed us to test a potential stress-protecting function of Var1. To this end, we grew cells that contained the MTS-Var1 plasmid or an empty plasmid as a control in the presence of chloramphenicol for 16 h before we exposed them to acute heat stress (Figure 3F). We observed that the expression of MTS-Var1 (whose expression levels are not affected by chloramphenicol) strongly protected cells from heat toxicity (Figure 3G). From this, we

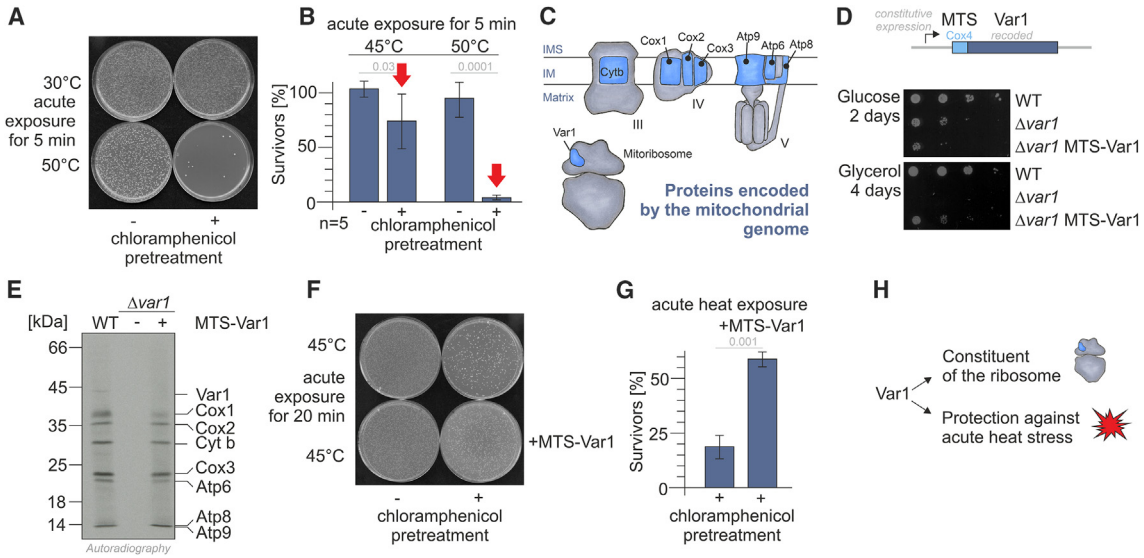

Figure 3. Mitochondrial protein synthesis protects against heat-induced proteotoxicity

(A and B) Wild-type cells were grown for 16 h at 30°C in galactose medium with or without 2 mg/mL chloramphenicol before they were exposed to 45°C or 50°C for 5 min. Aliquots were plated on glucose medium and counted from five biological replicates (mean ± SD).

(C) Schematic representation of the proteins encoded by the mitochondrial genome.

(D) The indicated strains were grown to log phase in galactose medium at 30°C. A total of 3 μL of the cell suspension was dropped onto glucose and glycerol plates, which were incubated at 30°C.

(E) Mitochondrial translation products were radiolabeled for 10 min at 30°C and visualized by autoradiography.

(F and G) Cells harboring an MTS-Var1 expression plasmid or an empty vector for control were treated as described in (A). The quantification shows results from three biological replicates (mean ± SD).

(H) Scheme to illustrate the two distinguishable activities of Var1.

conclude that Var1 plays a crucial role in stress protection. Importantly, this function is apparently independent from the role of Var1 as a structural element of the mitochondrial ribosome as it remains protective in cells lacking mitochondrial DNA and thus mitochondrial rRNAs (Figure 3H).

Var1 is a meta-stable protein with asparagine-rich unstructured segments

Var1 belongs to the S3 protein family, members of which are universal constituents of small ribosomal subunits.[47] In contrast to other S3 proteins, Var1 is extremely rich in asparagine residues (Figure 4A). More than 30% of all amino acid residues in the Var1 sequence are asparagine residues, making Var1 the most N-rich protein in the yeast genome (Figures 4B, S8A, and S8B). PolyN and polyQ proteins are well known for their aggregation-prone behavior.[48] While mitochondrially encoded Var1 homologs were consistently N-rich, nuclear-encoded S3 proteins (such as the mitochondrial S3 proteins of human cells) and bacterial S3 proteins have a low, ''normal'' asparagine content (Figure 4C; Table S1). Var1 contains three loop-forming segments that are not found in other S3 proteins (Figure S8C). These loops largely contribute to the high asparagine content of Var1 (blue regions in Figures 4A and 4D). The two longer loops L1 and L3 are each dispensable for mitochondrial protein synthesis, suggesting that these loops might have a translation-independent function (Figures S8D–S8G).

We next tested the aggregation behavior of Var1 directly. To this end, we performed *in organello* translation experiments, during which mitochondrial translation products were radiolabeled. Subsequently, we lysed the mitochondria and separated soluble from aggregated proteins by centrifugation (Figure 4E). In non-stressed cells, Var1 was soluble; however, in cells with compromised mitochondrial Hsp70, in those lacking the Pim1 protease or the Hsp78, a large fraction of Var1 was found in the pellet, indicating its aggregation (Figures 4E and S9A). Exposure of mitochondria to higher temperature also induced aggregation of Var1, but not that of other translation products (Figure 4F). Similarly, the expression of the misfolded mtCPY* protein induced Var1 aggregation (Figure 4G). Using the possibility to express Var1 as a nuclear-encoded protein (Figures S9B–S9D), we constructed fusions of MTS-Var1 with mScarlet (Figure 4H) or with GFP (Figure S9E), which clearly confirmed the heat-induced aggregation of Var1.

In summary, Var1 is an N-rich protein that forms intramitochondrial aggregates under stress conditions. In the following we refer to these Var1 aggregates as Var1 bodies.

Expression of the nuclear-encoded MTS-Var1 induces a strong mitoprotein-induced stress response

Why is Var1 mitochondrially encoded when it can be productively imported into mitochondria? To answer this question, we analyzed the consequences of expressing MTS-Var1 in wild-type cells with a normal, Var1-expressing mitochondrial genome. This allowed us to study the consequences of nuclear Var1 expression independently of its effects on mitochondrial gene expression. Expression of MTS-Var1 strongly impaired

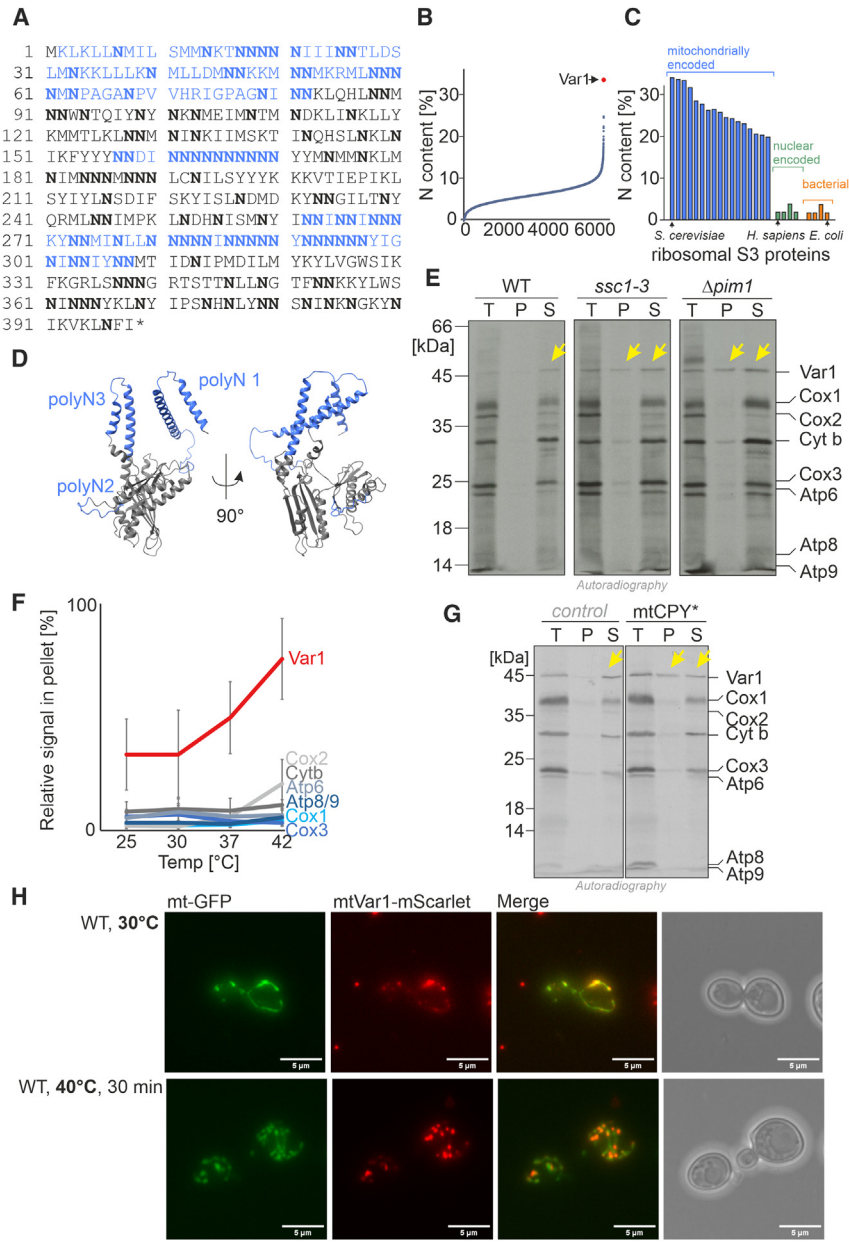

Figure 4. Var1 is a polyN protein with aggregation-prone nature

(A) Primary structure of Var1. Insertions that are not present in bacterial S3 proteins are highlighted in blue.

(B) The relative content of asparagine residues was calculated for all yeast proteins.[49]

(C) The asparagine content in Var1 and other S3 proteins was calculated. See Table S1 for details.

(D) The structure of Var1 was predicted by alpha fold.[50] The three loops shown in blue are only found in mitochondrially encoded S3 proteins (cf. Figure S8C). The figure was made with ChimeraX.[51]

(E) Mitochondria were isolated from wild-type, *ssc1-3*, and *Δpim1* mutants. Mitochondria were preincubated for 10 min at 33°C before mitochondrial translation products were radiolabeled for 20 min at 25°C. Samples were either directly analyzed (T, total) or separated into pellet (P) and soluble (S) fractions by centrifugation.

(F) Mitochondrial translation products were radiolabeled at different temperatures. Protein amounts in the pellet fraction relative to the total samples were quantified from three biological replicates. Error bars show standard deviations.

(G) Mitochondria were isolated from cells harboring plasmids for the expression of mtCPY* or empty plasmids for control. Mitochondrial translation products were analyzed as described for (E) after incubation at 25°C.

(H) Wild-type cells were transformed with mtGFP and an inducible MTS-Var1-mScarlet under control of an inducible *GAL* promotor. Cells were grown in raffinose medium, with additional 0.5% galactose for 4 h. After the expression was stopped, cells were shifted to 40°C for 30 min and analyzed by microscopy.

cell growth (Figures 5A and 5B). The toxicity of Var1 was independent of the presequence, as expression of Var1 in the cytosol was likewise toxic. On the contrary, expression of the bacterial S3 protein of *Escherichia coli* (*Ec*S3), an S3 variant of normal asparagine content, was not toxic, neither when expressed in the cytosol nor when it was targeted to mitochondria by fusion to the presequence. Expression of other mitochondrial ribosomal proteins, such as Mrps24, also had no toxic effect. Thus, nuclear expression of yeast Var1 severely compromises cellular viability.

To better characterize the consequences of MTS-Var1 expression, we analyzed the induction of stress response pathways (Figure 5C). Expression of MTS-Var1 induced the synthesis of *RPN4* mRNA, indicative of mitoprotein-induced stress.[12,53] Rpn4 induction increases the proteolytic activity of yeast cells, a hallmark of UPRam.[54,55] We also detected highly induced levels of *CIS1*, particularly in *rho*^{0} cells (Figure 5C). Cis1 is the primary target of the mitoCPR response,[56] which, upon induction under stress conditions, recruits the AAA extractor Msp1 to the TOM complex to remove stalled import intermediates.[57,58] The induction of Cis1 is indicative of a strong effect of MTS-Var1 as a clogger of the import machinery. The strong induction of the mitoCPR stress response was also supported by a reporter assay, which measures the expression of YFP under control of a pleotropic drug reporter element, the promoter segment that controls *CIS1* induction (Figure 5D). *In vitro*, radiolabeled MTS-Var1 was barely import competent (Figure S9F), and short preincubation times rendered the protein import incompetent, presumably owing to its aggregation-prone nature (Figure S9G). Nevertheless, the expression of MTS-Var1, in contrast to that of the b_2-DHFR clogger protein,[53] did not lead to the accumulation of mitochondrial precursor proteins in the cytosol (Figures 5E and 5F). In summary, we observed that its inherent aggregation-prone nature

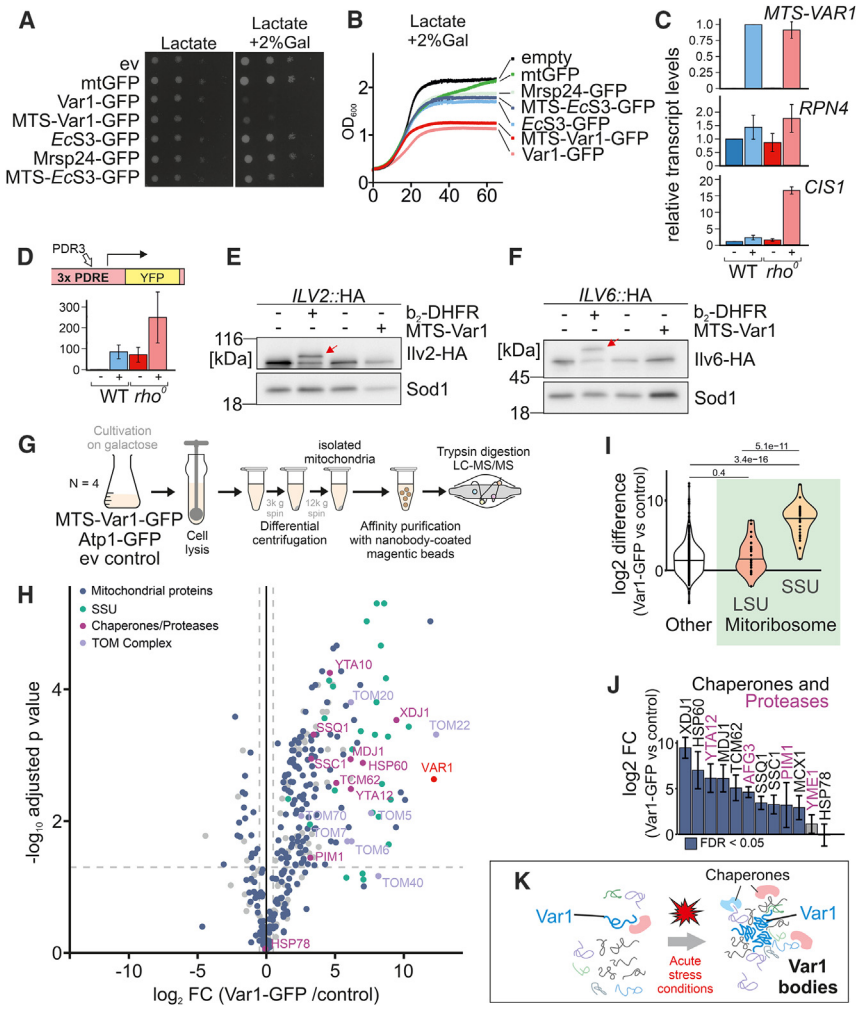

Figure 5. Nuclear expression of Var1 leads to clogging of the TOM complex and triggers the mitoprotein-induced stress response

(A) The proteins indicated were expressed in wild-type cells from a galactose-inducible promoter. Ten-fold serial dilutions of lactate-grown precultures were dropped onto the indicated plates and further incubated at 30°C.

(B) The growth of the cells shown in (A) was analyzed in a spectrometer under constant agitation.

(C) The indicated strains were grown on galactose medium at 30°C to exponential phase. The levels of the indicated mRNAs were measured from cell extracts by RT-qPCR. $n = 3$, mean ± SD.

(D) The response from the pleiotropic drug response element was measured in the different strains using a genetically encoded sensor.[52] $n = 3$, mean ± SD.

(E and F) Ilv2-HA or Ilv6-HA cells expressing the clogger protein b_2-DHFR or MTS-Var1 were grown on galactose medium before whole-cell extracts were prepared and analyzed by western blotting with HA- or Sod1-specific antibodies.

(G) Scheme of the detection of Var1 interactors by mass spectrometry.

(H) Proteins identified with MTS-Var1-GFP or control cells were detected. The volcano plot shows the proteins co-isolated with Var1 on the right-hand side. The positions of chaperones and TOM subunits are indicated.

(I) Violin plot showing the relative enrichment (log_2 fold change) of different protein groups with the MTS-Var1-GFP over the control sample.

(J) Enrichment of mitochondrial chaperones and proteases with Var1-GFP over control. The IMS protease Yme1 and Hsp78 were not recovered with Var1.

(K) Scheme showing the chaperone-binding to Var1.

strongly limits the import competence of Var1 and, together with the associated toxicity, explains why the *VAR1* gene remained in the mitochondrial genome, even though the productive targeting to mitochondria of Var1 per se is possible.

Next, we identified Var1 interactors within isolated mitochondria by purification of MTS-Var1-GFP with magnetic GFP Traps. Extracts from *Δvar1* mitochondria and wild-type mitochondria from Atp1-GFP-expressing cells served as controls (Figure 5G). The interactome of Var1 was highly enriched for proteins of the small subunit of the mitochondrial ribosome (Figures 5H and 5I; Table S1), confirming the productive assembly of the nuclear-encoded MTS-Var1 protein into the ribosome. Proteins of the large subunit were also recovered, however, to a lesser extent. In addition, the MTS-Var1-GFP efficiently co-isolated subunits of the TOM complex (Tom5, Tom6, Tom7, Tom20, and Tom22), while none of these was recovered with the Atp1-GFP or empty vector control. This clearly confirms the tight association of MTS-Var1-GFP with the import pore. Intriguingly, MTS-Var1-GFP also recovered a third group of proteins, namely mitochondrial chaperones and proteases (Figures 5H and 5J; Table S1). Basically, the whole complement of chaperones was recovered with MTS-Var1-GFP, including the mitochondrial Hsp70 proteins Ssc1 and Ssq1, the J protein for matrix protein folding Mdj1, and the chaperonin Hsp60, as well as the poorly characterized chaperones Tcm62 and Mcx1. Also, the Pim1 and the mAAA protease of the inner membrane with its subunits Yta10/Afg3 and Yta12, co-purified with MTS-Var1-GFP. Interestingly, Hsp78 was not recovered with MTS-Var1-GFP, suggesting that Hsp78 and Var1 do not physically interact. The strong association with import components and chaperones were not just the consequence of its folding in the matrix, as it was not seen for other proteins such as Atp1[59] (Figures S9H and S9I; Table S1).

Thus, in summary, our data show that Var1 is a highly aggregation-prone protein, which is difficult to import and, once it reaches the matrix, interacts with many components of the mitochondrial proteostasis network (Figure 5K).

The mitochondrial matrix contains two distinct types of stress-induced protein aggregates

The observed aggregation propensity of Var1, its interaction with chaperones and proteases, and its ability to protect *rho*^{0} cells

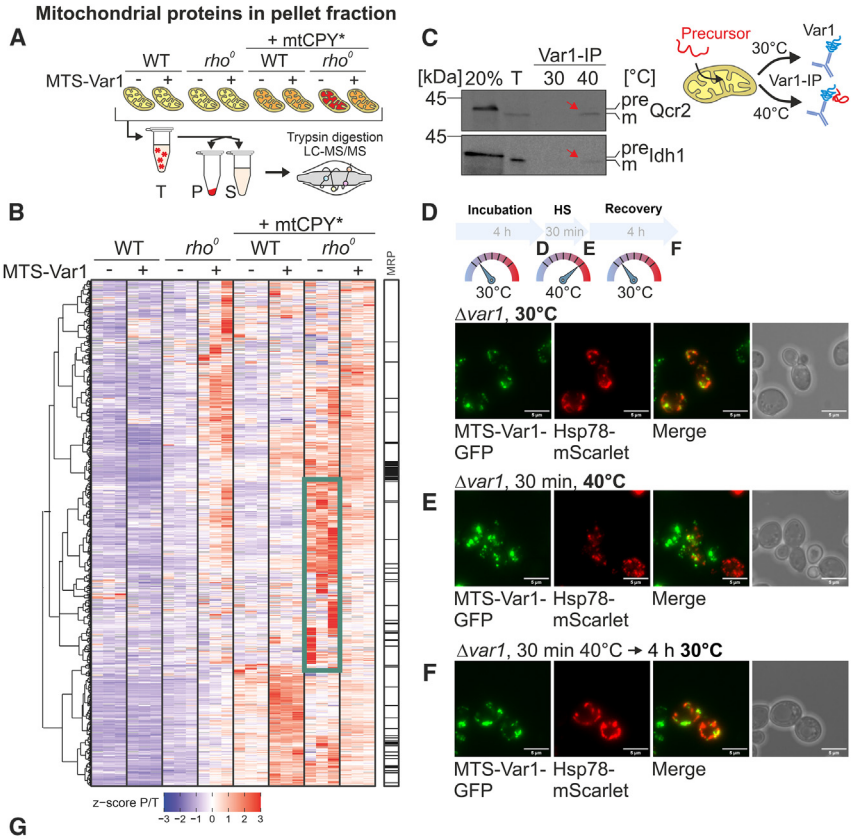

Figure 6. Var1 bodies are distinct from other Hsp78-bound aggregates

(A) Scheme of the proteomic assessment of aggregated proteins in mitochondria of wild-type and *rho*^{0} cells that express mtCPY* and MTS-Var1.

(B) Var1-dependent mitochondrial protein aggregation in response to proteotoxic stress. Heatmap of *Z* scored ratios between pellet and total protein abundance for mitochondrial proteins. Proteins are ordered based on ward D clustering using Euclidian distances. Mitochondrial ribosomal proteins (MRPs) are indicated. The green box indicates a group of proteins whose aggregation is suppressed in the presence of Var1. See also Dataset S1.

(C) Radiolabeled Qcr2 and Idh1 were incubated for 10 min with wild-type mitochondria. The import was stopped by depletion of the membrane potential. Mitochondria were split into two aliquots that were incubated at either 30°C or 40°C for 30 min. The samples were shifted to ice, and non-imported proteins were removed by protease treatment for 30 min. Mitochondria were lysed and Var1 was purified by immunoprecipitation (Var1-IP). The total (T) represents one-third of the amount of imported protein used per immunoprecipitation reaction.

(D–F) *Δvar1* cells expressing MTS-Var1-GFP (*TEF* promoter) and Hsp78-mScarlet (*TPI* promoter) were grown at 30°C (D) and transiently exposed to a short heat shock at 40°C for 30 min (E). Subsequently, cells were brought back to 30°C and further grown for 4 h (F).

(G) Model for the Var1-induced aggregate formation in mitochondria.

against acute heat stress resemble the features that are known for the polyQ protein Rnq1 and other aggregate-nucleating factors of the cytosol[60,61]: they absorb and buffer misfolded proteins during transient periods of proteotoxic insults. This stimulated us to test whether the presence of Var1 influences the mitochondrial proteome even in cells that lack a mitochondrial genome and thus mitochondrial ribosomes. To this end, we grew wild-type and *rho*^{0} cells that contained an MTS-Var1 expression plasmid or an empty plasmid for control, on galactose-based medium. Galactose allows the growth of the cells by fermentation but, unlike glucose, does not repress mitochondrial proteins.[62] Cellular extracts from four biological replicates were subjected to mass spectrometry (Figure S10A). The expression of MTS-Var1 left a characteristic footprint on the proteomes of these cells (Figure S10B): in both strains, the expression of MTS-Var1 increased the relative abundance of mitochondrial proteins in these cells (Figures S10C and S10D). This was particularly pronounced in *rho*^{0} cells, even though these cells do not contain functional mitochondrial ribosomes due to the absence of mitochondria rRNA. This shows that the ribosome-independent function of Var1 increases mitochondrial biogenesis (Figure S10E).

We directly assessed the influence of Var1 on the protein content of mitochondrial aggregates by the expression of mtCPY* to induce aggregate formation using wild-type and *rho*^{0} strains that lacked or expressed MTS-Var1 (Figures 6A and S11A). We isolated mitochondria from these strains, lysed them, and separated soluble and aggregated fractions by centrifugation. The protein content of these fractions (total, soluble, and aggregated) was analyzed by mass spectrometry in three independent replicates each (Figures S11B–S11F). As shown in the heatmap presented in Figure 6B, the expression of mtCPY* increased the amount of proteins in the pellet fraction (relative to the total protein), particularly in the *rho*^{0} background. The expression of MTS-Var1, however, suppressed the aggregation of many proteins (Figures 6B, green box, S11E, and S11F; Table S1; Dataset S1). Thus, Var1 expression stabilizes the mitochondrial proteome against proteotoxic stress.

To confirm that endogenous untagged Var1 interacts with matrix proteins under stress conditions we selected two matrix proteins whose aggregation behavior was found to be altered upon MTS-Var1 expression and which were found to be interactors of MTS-Var1-GFP, Idh1, and Qcr2. We synthesized radiolabeled precursors of these proteins and imported them into wild-type

mitochondria. We stopped the import reaction, incubated the mitochondria at 30°C or 40°C for 30 min before we isolated Var1 by immunoprecipitation. In both cases, the imported protein was recovered with Var1 after the heat shock, but not when mitochondria had been incubated at 30°C, indicating that Var1 binds to matrix proteins upon stress conditions (Figure 6C).

Finally, we tested whether the Var1 bodies are of transient nature and resolved once cells recover from stress conditions. We grew cells lacking the gene for mitochondrially encoded Var1 expressing MTS-Var1-GFP and Hsp78-mScarlet both expressed from constitutive promoters at 30°C. Hsp78 was predominantly dispersed and showed a uniform distribution in mitochondria, whereas MTS-Var1 was largely part of punctate foci (Figure 6D). Both proteins did not co-localize. Then, we shifted the cells to 40°C for 30 min, which induced the formation of Hsp78-bound aggregates (Figures 6E and S10F). Most of the Hsp78-positive aggregates were distinct from Var1 bodies, showing that Hsp78 also binds client proteins that are not associated with Var1. When we reduced the temperature back to 30°C, Var1 maintained its punctate distribution, whereas most of the Hsp78 dispersed again (Figure 6F). Two conclusions can be drawn from this experiment: first, the Var1 bodies represent a subfraction of mitochondrial protein aggregates and second, Var1 bodies are stable whereas other Hsp78-bound aggregates are transient and are resolved under favorable conditions. We conclude that the activity of Hsp78 as a disaggregase directly promotes the release of aggregated proteins from these transient aggregates (Figure 6G).

DISCUSSION

The controlled induction of protein aggregates serves as a strategy to sequester potentially harmful proteins.[2,63] Well-studied examples are inclusion bodies in bacteria, and it is well established that the formation of these amorphous aggregates considerably reduces protein toxicity.[63–65] Chaperones of the Hsp100, Hsp70, and Hsp60 protein families, such as ClpB, GroEL, and DnaK, do not prevent inclusion body formation in the first place, but were shown to dissemble these aggregates by releasing their proteins.[66–69]

The formation of intra-mitochondrial aggregates has been reported in the past,[8,11,28,70,71] but their relevance for mitochondrial proteostasis has remained largely elusive so far. We identified the mitochondrially encoded protein Var1 as a crucial component of the mitochondrial proteostasis network. Var1 has an extremely high asparagine content and, like other polyN and polyQ proteins, shows a high propensity to aggregate. Mutants of mitochondrial chaperones are known to induce the aggregation of newly synthesized Var1, a phenomenon that was observed in strains deficient in the matrix Hsp70 protein Ssc1,[72] in the matrix J protein Mdj1,[73] and in the chaperonins Hsp60[74] and Tcm62.[19,75] Ssc1 and Mdj1 thereby directly interact with newly synthesized Var1, maintain it soluble, and facilitate its assembly into the small subunit of mitochondrial ribosomes.[72,73] The expression of Var1 is under control of its specific mitochondrial translational activator Sov1, which also promotes Var1 assembly.[19] Var1 is synthesized at relatively high levels, exceeding the amounts required for mitoribosome biogenesis, and Ssc1 and Mdj1 are required to keep the super-stochiometric Var1 soluble.[19,72] Stress conditions presumably recruit the chaperones to other binding sites, thereby inducing Var1 aggregation (Figure 6G). As we show here, this gives rise to the formation of Var1 bodies that might sequester other misfolded, meta-stable or orphaned proteins.

The profound aggregation propensity of Var1 explains why the *VAR1* gene was not transferred to the nuclear genome. We generally found the high asparagine content in mitochondrially encoded S3 proteins, but not in species in which the gene is present on the nuclear genome (Figure 4C).[76] It therefore seems unlikely that mammalian cells use their mitoribosomal S3 protein as a nucleation factor for aggregate formation; another non-ribosomal protein presumably plays an analogous function here.

The use of tagged versions of Hsp78 and Var1 allowed us to distinguish two different types of aggregates. Whereas Var1 bodies were stable under the conditions we tested, other Hsp78-bound aggregates disappeared after the stress conditions had vanished. The stability of Hsp78-bound aggregates thereby depended on the stability of their substrates. The induction of mtCPY* resulted in permanent aggregates, presumably owing to the intrinsically misfolded nature of the protein.[31] However, exposure to a short heat shock at 40°C resulted in transient Hsp78-bound aggregates, consistent with previous reports.[10,28] In mitochondria of *rho*^{0} cells, which cannot assemble ribosomes due to the absence of rRNA, many of the orphaned mitoribosomal proteins were recovered with Hsp78. This suggests that non-assembled proteins serve as Hsp78 substrates even under non-stress conditions.

In the presence of Hsp78 only few mitochondrial proteins were bound to the non-catalytic mutant of Pim1. However, in *Δhsp78* mutants, the number of Pim1-bound proteins was strongly increased, suggesting that sequestration or refolding by Hsp78 and degradation by Pim1 are competing outcomes of protein misfolding in mitochondria. It has been reported before that the Pim1-mediated degradation of model substrates is slowed in *Δhsp78* mitochondria.[77] From this, it was proposed that Hsp78 promotes protein degradation via Pim1. However, it is also possible that the decreased degradation of the tested model substrate is due to the competition with other substrates that bind to Pim1 in *Δhsp78* mitochondria. In addition to substrates on Pim1, we found a number of proteins that efficiently co-eluted with Pim1, such as Mam33, Mrx6, and Pet20. These three proteins were recently reported to be permanent complex partners of Pim1 and involved in controlling the copy number of mitochondrial genomes.[78] Interestingly, we found two additional proteins similarly enriched: Sue1, a protein required for the degradation of the IMS protein cytochrome c,[79] and Rpo41, the mitochondrial RNA polymerase. The interaction of Pim1 with the RNA polymerase is unexpected and exciting, as it could explain the crucial role of Pim1 in mitochondrial genome stability.[24,42] This function of Pim1 seems to be conserved since a recent genome-wide study showed that single-point mutants and indels in the Pim1 gene are critical determinants for the mitochondrial DNA copy number in humans.[80] It will be exciting to study the relevance of this Pim1-Rpo41 complex in the future.

In general, the situation in the mitochondrial matrix resembles the situation known from the yeast cytosol: Hsp78, similar to Hsp104, binds to aggregates that can have a transient or stable nature.[5,14,16] It promotes the disassembly of these structures, if possible. The polyN protein Var1 serves as a nucleation factor for stable aggregates and thus seems to have an analogous role to Rnq1, which serves as a prion that controls aggregate formation as an extra-genetically inheritable trait.[81] Interestingly, such inheritable mitochondrial aggregates were recently described and named DUMPs (deposits of unfolded mitochondrial proteins).[11] These DUMPs were not molecularly characterized but it seems likely that they are identical to the Var1 bodies we identified here. It will be exciting to study the role of induced protein aggregates in detail in the future.

Limitations of the study

Var1 is a mitochondrially encoded protein. The mitochondrial genome cannot be easily manipulated, and genetically modified mitochondrial DNA is often unstable. This is why we used the nuclear encoded MTS-Var1 and GFP-tagged versions of it. We cannot exclude that the differences in Var1 biogenesis and potential stalling during the import of MTS-Var1 might influence some of the results of this study.

STAR★METHODS

Detailed methods are provided in the online version of this paper and include the following:

- KEY RESOURCES TABLE
- RESOURCE AVAILABILITY
  - Lead contact
  - Materials availability
  - Data and code availability
- EXPERIMENTAL MODEL AND STUDY PARTICIPANT DETAILS
  - Yeast strains, plasmids and growth conditions
- METHOD DETAILS
  - Growth assays and viability tests
  - YFP reporter assays
  - Cell lysates
  - Antibodies
  - Analysis of mRNA levels by qRT-PCR
  - Isolation of mitochondria
  - Localization of matrix proteins
  - Protein import into mitochondria
  - Radioactive *in vivo* labeling of mitochondrial translation products
  - Co-immunoprecipitations after import
  - Radioactive *in organello* labeling of mitochondrial translation products
  - Determination of aggregated translation products in mitochondria
  - Sample preparation and mass spectrometric identification of proteins
  - Analysis of mass spectrometry data
  - Fluorescence microscopy
- QUANTIFICATION AND STATISTICAL ANALYSIS

SUPPLEMENTAL INFORMATION

Supplemental information can be found online at https://doi.org/10.1016/j.celrep.2024.114018.

ACKNOWLEDGMENTS

We thank Sabine Knaus for technical assistance, Nikita Gupta for the Ilv2-HA and Ilv6-HA strains, and Timo Mühlhaus for the analysis of the N and Q content of yeast proteins. We thank Thomas Langer for the Hsp78 antibody and the *Δpim1* mutant strain. We are grateful to Pierce Hoenigman for critical reading of the manuscript. This project was supported by grants from the European Research Council (ERC 101052639 MitoCyto to J.M.H.), the Deutsche Forschungsgemeinschaft (HE2803/9-2 and GRK2737-STRESSistance to J.M.H. and Z.S.), and the Landesforschungsinitiative Rheinland-Pfalz BioComp (to Z.S. and J.M.H.).

AUTHOR CONTRIBUTIONS

L.B. constructed the strains and performed the biochemical, proteomic, microscopic, and yeast genetics experiments. M.R. and Z.S. carried out the mass spectrometry analysis and, together with J.-E.B., C.K., and L.B. analyzed the proteomics data. J.M.H. conceived and supervised the study. L.B. and J.M.H. wrote the manuscript, with all authors critically reviewing it.

DECLARATION OF INTERESTS

The authors declare no competing interests.

Received: October 2, 2023
Revised: February 27, 2024
Accepted: March 14, 2024
Published: March 28, 2024

REFERENCES

1. Labbadia, J., and Morimoto, R.I. (2015). The biology of proteostasis in aging and disease. Annu. Rev. Biochem. *84*, 435–464. https://doi.org/10.1146/annurev-biochem-060614-033955.
2. Sontag, E.M., Samant, R.S., and Frydman, J. (2017). Mechanisms and Functions of Spatial Protein Quality Control. Annu. Rev. Biochem. *86*, 97–122. https://doi.org/10.1146/annurev-biochem-060815-014616.
3. Spokoini, R., Moldavski, O., Nahmias, Y., England, J.L., Schuldiner, M., and Kaganovich, D. (2012). Confinement to organelle-associated inclusion structures mediates asymmetric inheritance of aggregated protein in budding yeast. Cell Rep. *2*, 738–747. https://doi.org/10.1016/j.celrep.2012.08.024.
4. Grousl, T., Ungelenk, S., Miller, S., Ho, C.T., Khokhrina, M., Mayer, M.P., Bukau, B., and Mogk, A. (2018). A prion-like domain in Hsp42 drives chaperone-facilitated aggregation of misfolded proteins. J. Cell Biol. *217*, 1269–1285. https://doi.org/10.1083/jcb.201708116.
5. Hill, S.M., Hao, X., Liu, B., and Nyström, T. (2014). Life-span extension by a metacaspase in the yeast Saccharomyces cerevisiae. Science *344*, 1389–1392. https://doi.org/10.1126/science.1252634.
6. Sontag, E.M., Morales-Polanco, F., Chen, J.H., McDermott, G., Dolan, P.T., Gestaut, D., Le Gros, M.A., Larabell, C., and Frydman, J. (2023). Nuclear and cytoplasmic spatial protein quality control is coordinated by nuclear-vacuolar junctions and perinuclear ESCRT. Nat. Cell Biol. *25*, 699–713. https://doi.org/10.1038/s41556-023-01128-6.
7. Adriaenssens, E., Asselbergh, B., Rivera-Mejías, P., Bervoets, S., Vendredy, L., De Winter, V., Spaas, K., de Rycke, R., van Isterdael, G., Impens, F., et al. (2023). Small heat shock proteins operate as molecular chaperones in the mitochondrial intermembrane space. Nat. Cell Biol. *25*, 467–480. https://doi.org/10.1038/s41556-022-01074-9.

8. Poveda-Huertes, D., Matic, S., Marada, A., Habernig, L., Licheva, M., Myketin, L., Gilsbach, R., Tosal-Castano, S., Papinski, D., Mulica, P., et al. (2020). An Early mtUPR: Redistribution of the Nuclear Transcription Factor Rox1 to Mitochondria Protects against Intramitochondrial Proteotoxic Aggregates. Mol. Cell *77*, 180–188.e9. https://doi.org/10.1016/j.molcel.2019.09.026.

9. Iosefson, O., Sharon, S., Goloubinoff, P., and Azem, A. (2012). Reactivation of protein aggregates by mortalin and Tid1–the human mitochondrial Hsp70 chaperone system. Cell Stress Chaperones *17*, 57–66. https://doi.org/10.1007/s12192-011-0285-3.

10. Jaworek, W., Sylvester, M., Cenini, G., and Voos, W. (2022). Elucidation of the interaction proteome of mitochondrial chaperone Hsp78 highlights its role in protein aggregation during heat stress. J. Biol. Chem. *298*, 102494. https://doi.org/10.1016/j.jbc.2022.102494.

11. Ruan, L., McNamara, J.T., Zhang, X., Chang, A.C.C., Zhu, J., Dong, Y., Sun, G., Peterson, A., Na, C.H., and Li, R. (2020). Solid-phase inclusion as a mechanism for regulating unfolded proteins in the mitochondrial matrix. Sci. Adv. *6*, eabc7288. https://doi.org/10.1126/sciadv.abc7288.

12. Krämer, L., Dalheimer, N., Räschle, M., Storchová, Z., Pielage, J., Boos, F., and Herrmann, J.M. (2023). MitoStores: chaperone-controlled protein granules store mitochondrial precursors in the cytosol. EMBO J. *42*, e112309. https://doi.org/10.15252/embj.2022112309.

13. Liu, Q., Chang, C.E., Wooldredge, A.C., Fong, B., Kennedy, B.K., and Zhou, C. (2022). Tom70-based transcriptional regulation of mitochondrial biogenesis and aging. Elife *11*, e75658. https://doi.org/10.7554/eLife.75658.

14. Sanchez, Y., and Lindquist, S.L. (1990). HSP104 required for induced thermotolerance. Science *248*, 1112–1115. https://doi.org/10.1126/science.2188365.

15. den Brave, F., Cairo, L.V., Jagadeesan, C., Ruger-Herreros, C., Mogk, A., Bukau, B., and Jentsch, S. (2020). Chaperone-Mediated Protein Disaggregation Triggers Proteolytic Clearance of Intra-nuclear Protein Inclusions. Cell Rep. *31*, 107680. https://doi.org/10.1016/j.celrep.2020.107680.

16. Gates, S.N., Yokom, A.L., Lin, J., Jackrel, M.E., Rizo, A.N., Kendsersky, N.M., Buell, C.E., Sweeny, E.A., Mack, K.L., Chuang, E., et al. (2017). Ratchet-like polypeptide translocation mechanism of the AAA+ disaggregase Hsp104. Science *357*, 273–279. https://doi.org/10.1126/science.aan1052.

17. Krobitsch, S., and Lindquist, S. (2000). Aggregation of huntingtin in yeast varies with the length of the polyglutamine expansion and the expression of chaperone proteins. Proc. Natl. Acad. Sci. USA *97*, 1589–1594. https://doi.org/10.1073/pnas.97.4.1589.

18. Kaganovich, D., Kopito, R., and Frydman, J. (2008). Misfolded proteins partition between two distinct quality control compartments. Nature *454*, 1088–1095. https://doi.org/10.1038/nature07195.

19. Seshadri, S.R., Banarjee, C., Barros, M.H., and Fontanesi, F. (2020). The translational activator Sov1 coordinates mitochondrial gene expression with mitoribosome biogenesis. Nucleic Acids Res. *48*, 6759–6774. https://doi.org/10.1093/nar/gkaa424.

20. Terpstra, P., and Butow, R.A. (1979). The role of var1 in the assembly of yeast mitochondrial ribosomes. J. Biol. Chem. *254*, 12662–12669.

21. Sanchirico, M., Tzellas, A., Fox, T.D., Conrad-Webb, H., Periman, P.S., and Mason, T.L. (1995). Relocation of the unusual *VAR1* gene from the mitochondrion to the nucleus. Biochem. Cell. Biol. *73*, 987–995.

22. Chacinska, A., Koehler, C.M., Milenkovic, D., Lithgow, T., and Pfanner, N. (2009). Importing mitochondrial proteins: machineries and mechanisms. Cell *138*, 628–644.

23. Deshwal, S., Fiedler, K.U., and Langer, T. (2020). Mitochondrial Proteases: Multifaceted Regulators of Mitochondrial Plasticity. Annu. Rev. Biochem. *89*, 501–528. https://doi.org/10.1146/annurev-biochem-062917-012739.

24. Van Dyck, L., Neupert, W., and Langer, T. (1997). PIM1 protease essential for pre-mRNA splicing and translation in mitochondria. Science. submitted.

25. Levchenko, I., Smith, C.K., Walsh, N.P., Sauer, R.T., and Baker, T.A. (1997). PDZ-like domains mediate binding specificity in the Clp/Hsp100 family of chaperones and protease regulatory subunits. Cell *91*, 939–947. https://doi.org/10.1016/s0092-8674(00)80485-7.

26. Deville, C., Franke, K., Mogk, A., Bukau, B., and Saibil, H.R. (2019). Two-Step Activation Mechanism of the ClpB Disaggregase for Sequential Substrate Threading by the Main ATPase Motor. Cell Rep. *27*, 3433–3446.e4. https://doi.org/10.1016/j.celrep.2019.05.075.

27. Zhou, C., Slaughter, B.D., Unruh, J.R., Eldakak, A., Rubinstein, B., and Li, R. (2011). Motility and segregation of Hsp104-associated protein aggregates in budding yeast. Cell *147*, 1186–1196. https://doi.org/10.1016/j.cell.2011.11.002.

28. Vazquez-Calvo, C., Kohler, V., Höög, J.L., Büttner, S., and Ott, M. (2023). Newly imported proteins in mitochondria are particularly sensitive to aggregation. Acta Physiol. *238*, e13985. https://doi.org/10.1111/apha.13985.

29. Abeliovich, H., Zarei, M., Rigbolt, K.T.G., Youle, R.J., and Dengjel, J. (2013). Involvement of mitochondrial dynamics in the segregation of mitochondrial matrix proteins during stationary phase mitophagy. Nat. Commun. *4*, 2789. https://doi.org/10.1038/ncomms3789.

30. Teichmann, U., van Dyck, L., Guiard, B., Fischer, H., Glockshuber, R., Neupert, W., and Langer, T. (1996). Substitution of PIM1 protease in mitochondria by *Escherichia coli* Lon protease. J. Biol. Chem. *271*, 10137–10142.

31. Hiller, M.M., Finger, A., Schweiger, M., and Wolf, D.H. (1996). ER degradation of a misfolded luminal protein by the cytosolic ubiquitin-proteasome pathway. Science *273*, 1725–1728. https://doi.org/10.1126/science.273.5282.1725.

32. Benjamini, Y., and Hochberg, Y. (1995). Controlling the False Discovery Rate: A Practical and Powerful Approach to Multiple Testing. J. Roy. Stat. Soc. B *57*, 289–300.

33. Cox, J., and Mann, M. (2008). MaxQuant enables high peptide identification rates, individualized p.p.b.-range mass accuracies and proteome-wide protein quantification. Nat. Biotechnol. *26*, 1367–1372.

34. Cox, J., Neuhauser, N., Michalski, A., Scheltema, R.A., Olsen, J.V., and Mann, M. (2011). Andromeda: a peptide search engine integrated into the MaxQuant environment. J. Proteome Res. *10*, 1794–1805.

35. Janke, C., Magiera, M.M., Rathfelder, N., Taxis, C., Reber, S., Maekawa, H., Moreno-Borchart, A., Doenges, G., Schwob, E., Schiebel, E., and Knop, M. (2004). A versatile toolbox for PCR-based tagging of yeast genes: new fluorescent proteins, more markers and promoter substitution cassettes. Yeast *21*, 947–962.

36. Livak, K.J., and Schmittgen, T.D. (2001). Analysis of relative gene expression data using real-time quantitative PCR and the 2(-Delta Delta C(T)) Method. Methods *25*, 402–408.

37. Rappsilber, J., Mann, M., and Ishihama, Y. (2007). Protocol for micro-purification, enrichment, pre-fractionation and storage of peptides for proteomics using StageTips. Nat. Protoc. *2*, 1896–1906.

38. Ritchie, M.E., Phipson, B., Wu, D., Hu, Y., Law, C.W., Shi, W., and Smyth, G.K. (2015). limma powers differential expression analyses for RNA-sequencing and microarray studies. Nucleic Acids Res. *43*, e47.

39. Simakin, P., Koch, C., and Herrmann, J.M. (2023). A modular cloning (MoClo) toolkit for reliable intracellular protein targeting in the yeast Saccharomyces cerevisiae. Microb. Cell *10*, 78–87.

40. Stacklies, W., Redestig, H., Scholz, M., Walther, D., and Selbig, J. (2007). pcaMethods–a bioconductor package providing PCA methods for incomplete data. Bioinformatics *23*, 1164–1167.

41. Westermann, B., and Neupert, W. (2000). Mitochondria-targeted green fluorescent proteins: convenient tools for the study of organelle biogenesis in *Saccaromyces cerevisiae*. Yeast *16*, 1421–1427.

42. van Dyck, L., Neupert, W., and Langer, T. (1998). The ATP-dependent PIM1 protease is required for the expression of intron-containing genes

in mitochondria. Genes Dev. *12*, 1515–1524. https://doi.org/10.1101/gad.12.10.1515.

43. Schmitt, M., Neupert, W., and Langer, T. (1995). Hsp78, a Clp homologue within mitochondria, can substitute for chaperone functions of mt-hsp70. EMBO J. *14*, 3434–3444.
44. Arends, J., Griego, M., Thomanek, N., Lindemann, C., Kutscher, B., Meyer, H.E., and Narberhaus, F. (2018). An Integrated Proteomic Approach Uncovers Novel Substrates and Functions of the Lon Protease in Escherichia coli. Proteomics *18*, e1800080. https://doi.org/10.1002/pmic.201800080.
45. Botos, I., Melnikov, E.E., Cherry, S., Tropea, J.E., Khalatova, A.G., Rasulova, F., Dauter, Z., Maurizi, M.R., Rotanova, T.V., Wlodawer, A., and Gustchina, A. (2004). The catalytic domain of Escherichia coli Lon protease has a unique fold and a Ser-Lys dyad in the active site. J. Biol. Chem. *279*, 8140–8148. https://doi.org/10.1074/jbc.M312243200.
46. Yang, J., Song, A.S., Wiseman, R.L., and Lander, G.C. (2022). Cryo-EM structure of hexameric yeast Lon protease (PIM1) highlights the importance of conserved structural elements. J. Biol. Chem. *298*, 101694. https://doi.org/10.1016/j.jbc.2022.101694.
47. Graifer, D., Malygin, A., Zharkov, D.O., and Karpova, G. (2014). Eukaryotic ribosomal protein S3: A constituent of translational machinery and an extraribosomal player in various cellular processes. Biochimie *99*, 8–18. https://doi.org/10.1016/j.biochi.2013.11.001.
48. Fiumara, F., Fioriti, L., Kandel, E.R., and Hendrickson, W.A. (2010). Essential role of coiled coils for aggregation and activity of Q/N-rich prions and PolyQ proteins. Cell *143*, 1121–1135. https://doi.org/10.1016/j.cell.2010.11.042.
49. Cherry, J.M., Hong, E.L., Amundsen, C., Balakrishnan, R., Binkley, G., Chan, E.T., Christie, K.R., Costanzo, M.C., Dwight, S.S., Engel, S.R., et al. (2012). Saccharomyces Genome Database: the genomics resource of budding yeast. Nucleic Acids Res. *40*, D700–D705. https://doi.org/10.1093/nar/gkr1029.
50. Jumper, J., Evans, R., Pritzel, A., Green, T., Figurnov, M., Ronneberger, O., Tunyasuvunakool, K., Bates, R., Žídek, A., Potapenko, A., et al. (2021). Highly accurate protein structure prediction with AlphaFold. Nature *596*, 583–589. https://doi.org/10.1038/s41586-021-03819-2.
51. Pettersen, E.F., Goddard, T.D., Huang, C.C., Couch, G.S., Greenblatt, D.M., Meng, E.C., and Ferrin, T.E. (2004). UCSF Chimera–a visualization system for exploratory research and analysis. J. Comput. Chem. *25*, 1605–1612. https://doi.org/10.1002/jcc.20084.
52. Koch, C., Räschle, M., Prescianotto-Baschong, C., Spang, A., and Herrmann, J.M. (2023). The ER-SURF pathway uses ER-mitochondria contact sites for protein targeting to mitochondria. Preprint at bioRxiv. https://doi.org/10.1101/2023.08.10.552816.
53. Boos, F., Krämer, L., Groh, C., Jung, F., Haberkant, P., Stein, F., Wollweber, F., Gackstatter, A., Zöller, E., van der Laan, M., et al. (2019). Mitochondrial protein-induced stress triggers a global adaptive transcriptional programme. Nat. Cell Biol. *21*, 442–451. https://doi.org/10.1038/s41556-019-0294-5.
54. Xie, Y., and Varshavsky, A. (2001). RPN4 is a ligand, substrate, and transcriptional regulator of the 26S proteasome: a negative feedback circuit. Proc. Natl. Acad. Sci. USA *98*, 3056–3061. https://doi.org/10.1073/pnas.071022298.
55. Wrobel, L., Topf, U., Bragoszewski, P., Wiese, S., Sztolsztener, M.E., Oeljeklaus, S., Varabyova, A., Lirski, M., Chroscicki, P., Mroczek, S., et al. (2015). Mistargeted mitochondrial proteins activate a proteostatic response in the cytosol. Nature *524*, 485–488. https://doi.org/10.1038/nature14951.
56. Weidberg, H., and Amon, A. (2018). MitoCPR-A surveillance pathway that protects mitochondria in response to protein import stress. Science *360*, eaan4146. https://doi.org/10.1126/science.aan4146.
57. Wang, L., and Walter, P. (2020). Msp1/ATAD1 in Protein Quality Control and Regulation of Synaptic Activities. Annu. Rev. Cell Dev. Biol. *36*, 141–164. https://doi.org/10.1146/annurev-cellbio-031220-015840.
58. Rödl, S., and Herrmann, J.M. (2023). The role of the proteasome in mitochondrial protein quality control. IUBMB Life *75*, 868–879. https://doi.org/10.1002/iub.2734.
59. Song, J., Steidle, L., Steymans, I., Singh, J., Sanner, A., Böttinger, L., Winter, D., and Becker, T. (2023). The mitochondrial Hsp70 controls the assembly of the F(1)F(O)-ATP synthase. Nat. Commun. *14*, 39. https://doi.org/10.1038/s41467-022-35720-5.
60. Ho, C.T., Grousl, T., Shatz, O., Jawed, A., Ruger-Herreros, C., Semmelink, M., Zahn, R., Richter, K., Bukau, B., and Mogk, A. (2019). Cellular sequestrases maintain basal Hsp70 capacity ensuring balanced proteostasis. Nat. Commun. *10*, 4851. https://doi.org/10.1038/s41467-019-12868-1.
61. Douglas, P.M., Treusch, S., Ren, H.Y., Halfmann, R., Duennwald, M.L., Lindquist, S., and Cyr, D.M. (2008). Chaperone-dependent amyloid assembly protects cells from prion toxicity. Proc. Natl. Acad. Sci. USA *105*, 7206–7211. https://doi.org/10.1073/pnas.0802593105.
62. Morgenstern, M., Stiller, S.B., Lübbert, P., Peikert, C.D., Dannenmaier, S., Drepper, F., Weill, U., Höß, P., Feuerstein, R., Gebert, M., et al. (2017). Definition of a High-Confidence Mitochondrial Proteome at Quantitative Scale. Cell Rep. *19*, 2836–2852. https://doi.org/10.1016/j.celrep.2017.06.014.
63. Tyedmers, J., Mogk, A., and Bukau, B. (2010). Cellular strategies for controlling protein aggregation. Nat. Rev. Mol. Cell Biol. *11*, 777–788. https://doi.org/10.1038/nrm2993.
64. Carrió, M., González-Montalbán, N., Vera, A., Villaverde, A., and Ventura, S. (2005). Amyloid-like properties of bacterial inclusion bodies. J. Mol. Biol. *347*, 1025–1037. https://doi.org/10.1016/j.jmb.2005.02.030.
65. Ramón, A., Señorale-Pose, M., and Marín, M. (2014). Inclusion bodies: not that bad. Front. Microbiol. *5*, 56. https://doi.org/10.3389/fmicb.2014.00056.
66. Rinas, U., Hoffmann, F., Betiku, E., Estapé, D., and Marten, S. (2007). Inclusion body anatomy and functioning of chaperone-mediated in vivo inclusion body disassembly during high-level recombinant protein production in Escherichia coli. J. Biotechnol. *127*, 244–257. https://doi.org/10.1016/j.jbiotec.2006.07.004.
67. Avellaneda, M.J., Franke, K.B., Sunderlikova, V., Bukau, B., Mogk, A., and Tans, S.J. (2020). Processive extrusion of polypeptide loops by a Hsp100 disaggregase. Nature *578*, 317–320. https://doi.org/10.1038/s41586-020-1964-y.
68. Weber-Ban, E.U., Reid, B.G., Miranker, A.D., and Horwich, A.L. (1999). Global unfolding of a substrate protein by the Hsp100 chaperone ClpA. Nature *401*, 90–93. https://doi.org/10.1038/43481.
69. Mogk, A., Bukau, B., and Kampinga, H.H. (2018). Cellular Handling of Protein Aggregates by Disaggregation Machines. Mol. Cell *69*, 214–226. https://doi.org/10.1016/j.molcel.2018.01.004.
70. Vijayvergiya, C., Beal, M.F., Buck, J., and Manfredi, G. (2005). Mutant superoxide dismutase 1 forms aggregates in the brain mitochondrial matrix of amyotrophic lateral sclerosis mice. J. Neurosci. *25*, 2463–2470. https://doi.org/10.1523/JNEUROSCI.4385-04.2005.
71. Bruderek, M., Jaworek, W., Wilkening, A., Rüb, C., Cenini, G., Förtsch, A., Sylvester, M., and Voos, W. (2018). IMiQ: a novel protein quality control compartment protecting mitochondrial functional integrity. Mol. Biol. Cell *29*, 256–269. https://doi.org/10.1091/mbc.E17-01-0027.
72. Herrmann, J.M., Stuart, R.A., Craig, E.A., and Neupert, W. (1994). Mitochondrial heat shock protein 70, a molecular chaperone for proteins encoded by mitochondrial DNA. J. Cell Biol. *127*, 893–902.
73. Westermann, B., Gaume, B., Herrmann, J.M., Neupert, W., and Schwarz, E. (1996). Role of the mitochondrial DnaJ homologue Mdj1p as a chaperone for mitochondrially synthesized and imported proteins. Mol. Cell Biol. *16*, 7063–7071.
74. Horwich, A.L., Caplan, S., Wall, J.S., and Hartl, F.-U. (1992). Chaperonin-mediated protein folding. In Membrane Biogenesis and Protein Targeting, W. Neupert and R. Lill, eds. (Elsevier), pp. 329–337.

75. Klanner, C., Neupert, W., and Langer, T. (2000). The chaperonin-related protein Tcm62p ensures mitochondrial gene expression under heat stress. FEBS Lett. *470*, 365–369. https://doi.org/10.1016/s0014-5793(00)01322-3.

76. Bertgen, L., Mühlhaus, T., and Herrmann, J.M. (2020). Clingy genes: Why were genes for ribosomal proteins retained in many mitochondrial genomes? Biochim. Biophys. Acta Bioenerg. *1861*, 148275. https://doi.org/10.1016/j.bbabio.2020.148275.

77. Rottgers, K., Zufall, N., Guiard, B., and Voos, W. (2002). The ClpB homolog Hsp78 is required for the efficient degradation of proteins in the mitochondrial matrix. J. Biol. Chem. *277*, 45829–45837. https://doi.org/10.1074/jbc.M207152200.

78. Göke, A., Schrott, S., Mizrak, A., Belyy, V., Osman, C., and Walter, P. (2020). Mrx6 regulates mitochondrial DNA copy number in Saccharomyces cerevisiae by engaging the evolutionarily conserved Lon protease Pim1. Mol. Biol. Cell *31*, 527–545. https://doi.org/10.1091/mbc.E19-08-0470.

79. Wei, J., and Sherman, F. (2004). Sue1p is required for degradation of labile forms of altered cytochromes C in yeast mitochondria. J. Biol. Chem. *279*, 30449–30458. https://doi.org/10.1074/jbc.M403742200.

80. Gupta, R., Kanai, M., Durham, T.J., Tsuo, K., McCoy, J.G., Kotrys, A.V., Zhou, W., Chinnery, P.F., Karczewski, K.J., Calvo, S.E., et al. (2023). Nuclear genetic control of mtDNA copy number and heteroplasmy in humans. Nature *620*, 839–848. https://doi.org/10.1038/s41586-023-06426-5.

81. Halfmann, R., Jarosz, D.F., Jones, S.K., Chang, A., Lancaster, A.K., and Lindquist, S. (2012). Prions are a common mechanism for phenotypic inheritance in wild yeasts. Nature *482*, 363–368. https://doi.org/10.1038/nature10875.

82. Peleh, V., Zannini, F., Backes, S., Rouhier, N., and Herrmann, J.M. (2017). Erv1 of Arabidopsis thaliana can directly oxidize mitochondrial intermembrane space proteins in the absence of redox-active Mia40. BMC Biol. *15*, 106.

83. Lenhard, S., Gerlich, S., Khan, A., Rödl, S., Bökenkamp, J.E., Peker, E., Zarges, C., Faust, J., Storchova, Z., Räschle, M., et al. (2023). The Orf9b protein of SARS-CoV-2 modulates mitochondrial protein biogenesis. J. Cell Biol. *222*, e202303002.

84. Schlagowski, A.M., Knöringer, K., Morlot, S., Sánchez Vicente, A., Flohr, T., Krämer, L., Boos, F., Khalid, N., Ahmed, S., Schramm, J., et al. (2021). Increased levels of mitochondrial import factor Mia40 prevent the aggregation of polyQ proteins in the cytosol. EMBO J. *40*, e107913.

85. Hansen, K.G., Aviram, N., Laborenz, J., Bibi, C., Meyer, M., Spang, A., Schuldiner, M., and Herrmann, J.M. (2018). An ER surface retrieval pathway safeguards the import of mitochondrial membrane proteins in yeast. Science *361*, 1118–1122.

86. Gambill, B.D., Voos, W., Kang, P.J., Miao, B., Langer, T., Craig, E.A., and Pfanner, N. (1993). A dual role for mitochondrial heat shock protein 70 in membrane translocation of preproteins. J. Cell Biol. *123*, 109–117.

87. Tyanova, S., Temu, T., and Cox, J. (2016). The MaxQuant computational platform for mass spectrometry-based shotgun proteomics. Nat. Protoc. *11*, 2301–2319.

STAR★METHODS

KEY RESOURCES TABLE

REAGENT or RESOURCE	SOURCE	IDENTIFIER
Antibodies		
anti-Sod1	Johannes Herrmann lab	(Peleh et al., 2017)[82]
anti-Mam33	Johannes Herrmann lab	(Krämer et al., 2023)[12]
anti-Oxa1	Johannes Herrmann lab	(Peleh et al., 2017)[82]
anti-Act1	Johannes Herrmann lab	(Lenhard et al., 2023)[83]
anti-GFP	Johannes Herrmann lab	(Schlagowski et al., 2021)[84]
anti-Var1	Johannes Herrmann lab	This Paper
anti-Hsp78	Thomas Langer	(Schmitt et al., 1995)[43]
anti-Tom70	Johannes Herrmann lab	(Lenhard et al., 2023)[83]
Anti-Ilv5	Johannes Herrmann lab	(Hansen et al., 2018)[85]
Anti-Rabbit secondary antibody	BioRad	172-1019
anti-HA	Roche	12013819001
Chemicals, peptides, and recombinant proteins		
Sera-Mag Beads	Thermo Scientific	4515-2105-050250
Water, HPLC grade	Chromanorm	23595.294
0.2 M HEPES/NaOH pH 8.4	Sigma Aldrich	H3375
100% Ethanol, HPLC grade	VWR	153385E
Formic Acid, mass spectrometry grade	Sigma Aldrich	94318
Chloroacetamide	Sigma Aldrich	C0267
Trypsin	Promega	V5111
DMSO, HPLC grade	Sigma Aldrich	42780.AK
TMT10plex isobaric label reagent set	Thermo Scientific	90111
Acetonitrile	Honeywell	34967
Hydroxylamine	Sigma Aldrich	438227
Dithiothreitol	BioChemica	A1101,0025
Carbonyl cyanide 3-chlorophenylhydrazone	Sigma Aldrich	C2759-250MG
Anhydrotetracycline	Cayman chemical company	10009542
5′Fluorootic acid Monohydrate	US Biological	F5050
Cyclohexamide	AppliChem	A0879
Zymolyase-20T	Seikagaku Biobusiness	120491–1
Pyruvate Kinase	Roche	10109045001
Protease Inhibitor Cocktail, mini Tablet	MedChemExpress	HY-K0011
PhosSTOP™	Roche	4906845001
ChromoTek GFP-Trap® Magnetic Agarose	Chromotek	AB_2631357
monoclonal Anti-HA antibody	Sigma	22190322
Amintra Protein A Resin	Expedeon	APA0100
Trichloroacetic acid	Supelco	1.00807
Empore SPE-Scheiben	Supelco	66883-U
Empore SPE-Scheiben	Supelco	66886-U
Empore SPE-Scheiben	Supelco	66889-U
Guanidine hydrochloride	Sigma Aldrich	G3272
Lysyl endopeptidase	FUJIFILM	125–05061
Critical commercial assays		
Quick Coupled Transcription/Translation kit	Promega	L2080
RNeasy Mini Kit	Qiagen	74104

(*Continued on next page*)

Continued

REAGENT or RESOURCE	SOURCE	IDENTIFIER
RNase-Free DNase Set	Qiagen	79254
qScript cDNA Synthesis Kit	Quanta Biosciences	95047
iTaq Universal SYBR Green Supermix	BioRad	1725120
Pierce BCA Protein Assay Kit	Thermo Scientific	23225
TMT10plex isobaric label reagent set	Thermo Scientific	90111
Deposited data		
Mass spectrometry data: HSP78 AP-MS	This Paper	PRIDE: https://www.ebi.ac.uk/pride/archive/projects/PXD045196
Mass spectrometry data: PIM1 AP-MS (Project accession: PXD045286)	This Paper	PRIDE: https://www.ebi.ac.uk/pride/archive/projects/PXD045286
Mass spectrometry data: VAR1 AP-MS (Project accession: PXD045288)	This Paper	PRIDE: https://www.ebi.ac.uk/pride/archive/projects/PXD045288
Mass spectrometry data: Total proteome of NTS-VAR1 expressing yeast cells (Project accession: PXD045290)	This Paper	PRIDE: https://www.ebi.ac.uk/pride/archive/projects/PXD045290
Mass spectrometry data: TMT dataset of aggregates in mitochondria (Project accession: PXD048691)	This Paper	PRIDE: https://www.ebi.ac.uk/pride/archive/projects/PXD048691
Experimental models: Organisms/strains		
W303 *Δhsp78*: *hsp78Δ::NatNT2* derivative of W303	This study	N/A
Δvar1 MATa, *leu2-3,112 lys2 ura3-52 his3-ΔHindIII arg8::HISG*	Thomas D. Fox	(Sanchirico et al., 1995)[21]
ssc1-3 MATα; *ade2-101*, *lys2*, *ura3-52*, *leu2-3*, Δ*trp1* ssc1-3(LEU2) derivate of PK82	Herrmann Lab	(Gambill et al., 1993)[86]
YPH500 *Δpim1* SUP MATa *pim1::HIS3* (ρ^+) Yep13-SUP: 2μm LEU2derivate of YPH500	Herrmann Lab	(van Dyck et al., 1998)[42]
YPH499 MATa *ura3-52 lys2-801_amber ade2-101_ochre trp1-Δ63 his3-Δ200 leu2-Δ1 arg4::KanMX4* + pYX142 Hsp104-GFP + pYX233 cyt-DHFR derivative of YPH499 *Δarg4*	Herrmann Lab	(Krämer et al., 2023)[12]
W303 WT *rho*^{0}: MATα *leu2-3,112 trp1-1 can1-100 ura3-1 ade2-1 his3-11,15* [p^0]	This study	N/A
YPH499 MATa *ade2-101 his3-200 leu2-1 ura3-52 trp1-63 lys2-80 arg4::kanMX4 ilv2::HA* HIS3MX6 derivative of YPH499 *Δarg4*	Herrmann Lab	N/A
YPH499 MATa *ade2-101 his3-200 leu2-1 ura3-52 trp1-63 lys2-80 arg4::kanMX4 ilv6::HA* HIS3MX6 derivative of YPH499 *Δarg4*	Herrmann Lab	N/A
W303 *Δsov1*: *sov1Δ::NatNT*$_2$ derivative of W303	This study	N/A
W303 pNH605-PDRE-YFP derivative of W303	This study	N/A
W303 *rho*^{0} pNH605-PDRE-YFP derivative of W303	This study	N/A
Oligonucleotides		
See Table S1		
Software and algorithms		
Corel Technical Suite 2020	Corel	https://coreldraw.com
UCSF ChimeraX	Resource for Biocomputing, Visualization, and Informatics (RBVI)	(Pettersen et al., 2004)[51]
R 4.2.1	R Core Team	https://cran.r-project.org/
MaxQuant 2.0.1.0	N/A	(Tyanova et al., 2016)[87]
AIDA software	Elysia-raytest	https://www.aida.software/
Leica Application Suite X	Leica	https://www.leica-microsystems.com
ImageJ 1.54f	ImageJ	https://imagej.net/ij/

(*Continued on next page*)

Continued

REAGENT or RESOURCE	SOURCE	IDENTIFIER
MARS Data Analysis	BMG Labtech	https://www.bmglabtech.com
Image Lab 6.1	BioRad	https://www.bio-rad.com

RESOURCE AVAILABILITY

Lead contact

Further information and requests for resources and reagents should be directed to and will be fulfilled by the lead contact, Johannes M. Herrmann (hannes.herrmann@biologie.uni-kl.de).

Materials availability

All unique/stable reagents generated in this study are available from the lead contact without restriction.

Data and code availability

- All proteomic datasets obtained in this study have been deposited at to the ProteomeXchange Consortium via the PRIDE partner repository and are publicly available as of the date of publication. Accession numbers are listed in the key resources table.
- No original code has been generated.
- Any additional information required to reanalyze the data reported in this paper is available from the lead contact upon request.

EXPERIMENTAL MODEL AND STUDY PARTICIPANT DETAILS

Yeast strains, plasmids and growth conditions

The yeast strains used in this study are based on, W303, YPH499 or YPH500 background. All strains used in this study are described in detail in the key resource table. *Δhsp78* and *Δsov1* deletions were generated in W303 backgrounds by replacing the genomic reading frame with the natNT2 cassette (Janke et al., 2004). To select positive colonies, yeast transformants were plated on a selective Nat-containing media. The colonies for *hsp78* and *sov1* knockouts were verified by PCR.

ILV2 and *ILV6* were genomically tagged with 6HA and an *HIS3* cassette on the C terminus following the Janke et al. protocol to measure precursors upon stress. To select positive colonies, yeast transformants were plated on a selective synthetic histidine dropout medium. The colonies for tagged ILV2 and ILV6 were verified by PCR.

The strain lacking mtDNA (*rho0*) was generated by treatment of the wild-type strain (W303) with ethidium bromide (EtBr). Briefly, EtBr was added to a concentration of 10 μg/mL and the cells were incubated at 30°C, for approximately 24 h in YPD (1% yeast extract, 2% peptone, 2% dextrose). Following incubation with EtBr, the cells were diluted in water and plated on YPD to obtain single colonies. The *rho0* cells were selected as cells unable to grow on YPG (1% yeast extract, 2% peptone, 2% glycerol) plates, but can grow on YPD. In *rho0* cells, the loss of mtDNA was verified by qRT-PCR.

For the detection of the mitochondrial network, mScarletI was fused to the MTS of subunit 9 of the *Neurospora crassa* ATPase and the KanR-ColE1 cassette with the modular cloning (MoClo) toolkit (Simakin et al., 2023) and integrated into the YPRCΔ15 locus. To select positive colonies, yeast transformants were plated on a selective G418-containing media. The colonies were verified by microscopy. Alternatively, the plasmid pYX142-mtGFP (Westermann and Neupert, 2000) was employed. For the generation of Hsp78-GFP, pYX142 mtGFP was digested with EcoRI-HF and BamHI-HF, and the Hsp78 amplified without stop codon and matching overhangs to the vector to allow for Gibson Assembly using the Gibson Assembly Master Mix – Assembly (E2611) kit. Following the same approach, the carboxypeptidase Y CPY, the misfolding mutant version CPY* (G255R), or the misfolding mutant of the mouse dihydrofolate-reductase ($DHFR^{mut}$, C7S, S42C, N49C) without a stop codon were amplified and assembled into the pYX233-Su9-DHFR plasmid, digested using the restriction enzymes BamHI-HF and HindIII-HF. To generate the fluorophore tagged versions mScarletI was amplified. The resulting sequences were cloned into the pYX113 empty vector.

For the construction of MTS-Var1, the first 25 residues of the Cox4 flanked by the BamHI and EcoRI were annealed and, together with the PCR product of Var1 with EcoRI and SalI restriction sites, cloned into the digested pRS416 plasmid. GFP was amplified with SalI and XhoI and cloned into the same backbone where Var1 without a stop codon was used.

The Pim1 mutant S1015A was generated via the assembly of two PCR products generated with primers containing the point mutation, followed by subsequent assembly into the pYX142 plasmid digested with EcoRI.

For the generation of plasmids for the generation of radioactive lysate the pGem4 empty vector was digested with BamHI and HindIII. PCR products for Idh1 and Cor1 were digested and than assembled into the backbone. For the pGem4 MTS-Var1 the

Var1 was amplified including the Cox4-MTS from the p416 backbone and assembled into the pGem4 vector via the usage of EcoRI and SalI restriction sites.

To generate the truncations of Var1 lacking the different loops as indicated, PCR products were generated without the indicated regions. The products were assembled into the pYX142 empty vector digested with EcoRI and BamHI.

The strains were grown at 30°C either in yeast complete medium (YP) containing 1% (w/v) yeast extract, 2% (w/v) peptone and 2% (w/v) of the respective carbon source or in minimal synthetic respiratory medium containing 0.67% (w/v) yeast nitrogen base and 2% (w/v) of the respective carbon source. For expression of different proteins 0.5% galactose was added to the medium, or cells were pelleted and resuspended in galactose-containing medium.

METHOD DETAILS

Growth assays and viability tests

For spot analysis, the respective yeast strains were grown in liquid media. Yeast cells equivalent to 0.5 OD_{600} were harvested at the exponential phase. The cells were washed in sterile water and 3 μL of 10-fold serial dilutions were spotted on the respective media followed by incubation at 30°C. Pictures were taken after different days of the incubation.

Growth curves were performed in a 96 well plate, using the automated SPECTROstar^{Nano}- (BMG LabTech). The growth curves started at 0.1 OD_{600} and the OD_{600} was measured every 10 min for 72 h at 30°C. The mean of technical triplicates was calculated and plotted in R.

For survival assays cells were grown in liquid media and optional treated with chloramphenicol for 16 h before an acute heat treatment with the indicated temperatures. The same OD_{600} of cells were plated onto SD plates and colonies were counted.

For acute heat exposure cells were diluted into preheated media with the indicated temperatures before spotting onto plates or further use in growth curves.

YFP reporter assays

The PDRE-YFP reporter gene was integrated into the *LEU2* locus of the yeast genome. Cells were grown in galactose-containing media. 4 OD_{600} of cells were harvested by centrifugation (12,000 g, 5 min, RT) and resuspended in 400 μL H_2O. 100 μL of the cell suspension were transferred to flat-bottomed black 96-well imaging plates (BD Falcon, Heidelberg, Germany) in technical triplicates. Cells were sedimented by gentle spinning (30 g, 5 min, RT) and fluorescence (excitation 497 nm, emission 540 nm) was measured using a ClarioStar Fluorescence plate reader (BMG-Labtech, Offenburg, Germany). The corresponding wild-type strain not expressing YFP was used for background autofluorescence subtraction. Fluorescence intensities were normalized to the value obtained from the wild-type empty vector control in each of three independent biological replicates.

Cell lysates

For whole cell lysates, yeast strains were cultivated in liquid media to mid-log phase. 2 OD_{600} were harvested by centrifugation (12,000 g, 5 min) and resuspended in 100 μL reducing loading buffer. Cells were transferred to screw-cap tubes containing 1 mm glass beads. Cell lysis was performed using a FastPrep-24 5G homogenizer (MP Biomedicals, Heidelberg, Germany) with 3 cycles of 20 s, speed 6.0 m/s, 120 s breaks, glass beads. Lysates were boiled at 96°C for 5 min and stored at −20°C until further use. Equal amounts were resolved via SDS-PAGE.

Antibodies

The antibodies against Sod1, Mam33, Oxa1, Act1, GFP and Var1 were raised in rabbits using recombinant purified proteins. The antibody against Hsp78 was kindly gifted by Thomas Langer (Max Planck Institute for Biology and Aging, Germany). The horseradish peroxidase coupled HA antibody was ordered from Roche (Anti-HA-Peroxidase, High Affinity 3F10, #12 013 819 001). The secondary antibodies were ordered from Biorad (Goat Anti-Rabbit IgG (H + L)-HRP Conjugate #172–1019). Antibodies were diluted in 5% (w/v) nonfat dry milk-TBS (Roth T145.2) with the following dilutions: anti-Sod1 1:500, anti-GFP 1:5000 anti-Mam33 1:500, anti-Oxa1 1:500, anti-Var1 1:500, anti-Rabbit 1:10,000.

Analysis of mRNA levels by qRT-PCR

For total RNA extraction yeast strains were cultivated in synthetic media to mid-log phase. 4 OD_{600} of cells were harvested for RNA extraction using the RNeasy Mini Kit (Qiagen) in conjunction with the RNase-Free DNase Set (Qiagen) according to the manufacturer's instructions. Yield and purity of the obtained RNA was determined with a Spectrophotometer/Fluorometer DS-11 FX+ (DeNovix). 500 ng RNA were reverse transcribed into cDNA using the qScript cDNA Synthesis Kit (Quanta Bioscniences) according to the manufacturer's instructions. To measure relative mRNA levels, the iTaq Universal SYBR Green Supermix (BioRad) was used with 2 μL of a 1:10 dilution of cDNA sample. Measurements were performed in technical triplicates with the CFX96 Touch Real-Time PCR Detection System (BioRad). Calculations of the relative mRNA expressions were conducted following the 2-ΔΔCt method (Livak and Schmittgen, 2001). For normalization, the housekeeping gene *TFA2* was used due to its stability. See Table S1 for primer sequences.

Isolation of mitochondria

For the isolation of mitochondria, cells were grown in rich or selective galactose media to mid-log phase. Cultures with inducible genes were treated with 0.5% of galactose for 4 h. Cells were harvested (2,000 g, 5 min, RT) in the exponential phase. After a washing step, cells were treated for 10 min with 2 mL per g wet weight MP1 buffer (100 mM DTT, 10 mM Tris pH unadjusted) at 30°C. After washing with 1.2 M sorbitol, yeast cells were resuspended in 6.7 mL per g wet weight MP2 buffer (20 mM KPi buffer pH 7.4, 1.2 M sorbitol, 3 mg per g wet weight zymolyase 20T from Seikagaku Biobusiness) and incubated for 1 h at 30°C. Spheroplasts were collected via centrifugation at 4°C and resuspended in ice-cold homogenization buffer (13.4 mL/g wet weight) (10 mM Tris pH 7.4, 1 mM EDTA pH 8, 0.2% fatty acids free bovine serum albumin (BSA), 1 mM PMSF, 0.6 M sorbitol). Spheroplasts were disrupted by 10 strokes with a cooled glass potter. Cell debris was removed via centrifugation at 1,500 g for 5 min. The supernatant was centrifuged for 12 min at 12,000 g to collect mitochondria. Mitochondria were resuspended in 1 mL of ice-cold SH-buffer (0.6 M sorbitol, 20 mM HEPES pH 7.4). The mitochondria were diluted to a protein concentration of 10 mg/mL.

Localization of matrix proteins

The sublocalization of mitochondrial proteins was performed by hypoosmotic swelling and proteinase K digest. 10 μg of mitochondria were incubated either in SH buffer (0.6 M sorbitol, 20 mM HEPES pH 7.4) or hypotonic swelling buffer (60 mM sorbitol, 20 mM HEPES pH 7.4) for 30 min on ice in the absence or presence of 10 μg/mL proteinase K. Proteinase digestion was stopped by addition of SH buffer containing 2 mM PMSF. Mitochondria were pelleted by centrifugation and resuspended in 50 μL Laemmli buffer.

Protein import into mitochondria

The TNT Quick Coupled Transcription/Translation Kit from Promega was used for the synthesis of ^{35}S-methionine labeled proteins in reticulocyte lysate. 50 μg mitochondria were taken in import buffer (500 mM sorbitol, 50 mM HEPES pH 7.4, 80 mM KCl, 10 mM $Mg(OAc)_2$ and 2 mM KH_2PO_4), 2 mM ATP and 2 mM NADH and incubated for 10 min at 30°C. The import reaction was started by addition of 1% (v/v) reticulocyte lysate. To determine the lysate import capacity the lysate was diluted in SH-buffer and import directly started with the addition of isolated mitochondria. Samples were taken after the indicated time points and the reaction was stopped by a 1:10 dilution in ice-cold SH buffer supplemented with 100 μg/mL proteinase K. The samples were incubated on ice for 30 min to remove precursors which were not imported. The protease treatment was stopped by addition of 2 mM PMSF. The samples were centrifuged 15 min at 25,000 g and 4°C. The mitochondria were washed with 500 μL SH/KCl-buffer (0.6 M sorbitol, 20 mM HEPES/KOH pH 7.4, 150 mM KCl) and 2 mM PMSF. The mitochondria were reisolated by centrifugation for 15 min at 25,000 g and 4°C, resuspended in sample buffer and resolved via SDS-PAGE.

Radioactive *in vivo* labeling of mitochondrial translation products

Cells were grown in galactose medium lacking methionine to exponential phase. Aliquots of 2 OD were treated with 10 mg/mL cycloheximide to inhibit cytosolic translation. ^{35}S-methionine (1 μL of a 11 μCi solution) was added to the cell suspension and newly synthesized proteins were labeled for 10 min. The incorporation of radioactive methionine was quenched by the addition of 8 mM cold methionine. Cells were lysed with 0.3 M NaOH, 1% β-mercaptoethanol and 3 mM PMSF. Proteins were precipitated with 12% trichloroacetic acid and analyzed by SDS–PAGE and autoradiography.

Co-immunoprecipitations after import

Lysates for Cor1 and Idh1 were imported for 10 min as described above. Mitochondria were lysed (20 mM Tris-HCl, pH 7.4, 150 mM potassium chloride (KCl), 10 mM magnesium chloride, 5 mM EDTA, 1% Triton X-100, 2 mM PMSF, 40 U/ml apyrase) for 15 min, 4°C. The antibody against Var1 produced in rabbits and Amintra Protein A Resin (#APA0100) were mixed with the lysate and tumbled end-over-end for 1 h at 4°C. The supernatant was discarded, and beads were washed twice with wash buffer I (150 mM NaCl, 50 mM Tris-HCl, pH 7.5, 5% glycerol, 0.05% Triton X-100) and all samples twice with wash buffer (same as lysis buffer without the apyrase). Protein was eluted by the addition of sample buffer, and samples were boiled for 5 min at 96°C before SD-PAGE and autoradiography analyzed samples.

Radioactive *in organello* labeling of mitochondrial translation products

Isolated mitochondria (100 μg) were incubated in 1.5x *in organello* translation buffer (ioTL buffer, 20 mM HEPES/KOH pH 7.4, 15 mM KPi, 0.6 M sorbitol, 150 mM KCl, 12.66 mM $MgSO_4$, 12 μg/mL of all amino acid except methionine, 7.5 mM phosphoenolpyruvate, 6 mM ATP, 0.75 mM GTP, 5 mM α-ketoglutarate, 10 μg/mL pyruvate kinase) together with 1μL ^{35}S-methionine (of a 11 μCi solution) and incubated at 30°C for 10 min shaking at 600 rpm. Incorporation of radioactive methionine was quenched by the addition of 8 mM cold methionine and the reaction was stopped by the addition of 1 mL ice-cold SH buffer. Mitochondria were pelleted by centrifugation (20,000 g, 10 min, 4°C), resuspended in loading buffer and analyzed by SDS-PAGE and autoradiography.

Determination of aggregated translation products in mitochondria

Isolated mitochondria (100 μg) were resuspended in 1.5x ioTL buffer and incubated shaking (600 rpm, 10 min, 25°C or 33°C). Translation products were labeled for 15 min with 1 μL ^{35}S-methionine (of a 11 μCi solution). Incorporation of radioactive methionine was quenched by the addition of 25 mM methionine and the reaction was stopped by the addition of 1 mL ice-cold SH buffer. For the total

(T) samples, mitochondria were pelleted at 20,000 g for 10 min at 4°C, resuspended in loading buffer, and resuspended by shaking vigorously at 4°C for 5min. Aggregated and soluble protein fractions were obtained by mitochondrial lysis (0.1% Triton X-100, 150 mM NaCl, 5 mM EDTA, 1 mM PMSF) at 4°C for 15 min. To prevent sedimentation of ribosomes the samples were centrifuged at 30.000 g, 15 min 4°C. The pellet (P) fraction was prepared following the total samples and the proteins were precipitated with trichloroacetic acid.

Sample preparation and mass spectrometric identification of proteins

For the co-immunoprecipitation of interactors and mass spectrometry cells were grown in SGal media and 20 OD_{600} were harvested by centrifugation (12,000 g, 5 min) and snap-frozen in liquid nitrogen and stored at −80°C. Cell lysates were prepared in lysis buffer (50 mM Tris pH 7.5, 2% (w/v) SDS, Tablets mini EDTA-free protease inhibitor (Roche)) using a FastPrep-24 5G homogenizer (MP Biomedicals, Heidelberg, Germany) with 3 cycles of 30 s, speed 8.0 m/s, 120 s breaks, glass beads). For co-immunoprecipitation of Var1 mitochondria were isolated and 500 μg of protein was lysed (10 mM Tris-HCl, pH 7.5, 150 mM sodium chloride (NaCl), 0.5 mM EDTA, 10 mM magnesium chloride ($MgCl_2$), 0.5% Triton X-100, 1 mM PMSF) for 30 min, 4°C. Cleared lysates (20,000 g, 10 min, 4°C) were diluted with dilution buffer (10 mM Tris-HCl, pH 7.5, 150 mM NaCl, 0.5 Mm EDTA; 1x complete protease inhibitor cocktail, 1x PhosSTOP phosphatase inhibitor cocktail) and incubated with activated beads (ChromoTek GFP-Trap Magnetic Agarose; monoclonal Anti-HA antibody produced in mouse (Sigma #22190322) and Amintra Protein A Resin #APA0100) and tumbled end-over-end for 1 h at 4°C. The supernatant was discarded, and beads for $Pim1^{S1015}$-HA and MTS-Var1-eGFP were washed twice with wash buffer I (150 mM NaCl, 50 mM Tris-HCl, pH 7.5, 5% glycerol, 0.05% Triton X-100) and all samples twice with wash buffer II (150 mM NaCl, 50 mM Tris-HCl, pH 7.5, 5% glycerol). Peptides were digested on-bead with Elution buffer I (2 M urea, 50 mM Tris-HCl, pH 7.5, 1 mM DTT, 5 ng/μL trypsin (Promega, #V5111)) for 1 h at room temperature. 15 ng/μL fresh Trypsin was added for 10 min at room temperature. Eluted peptides were transferred to a fresh tube and incubated with 50 μL elution buffer (2M urea, 50 mM Tris-HCl, pH 7.5, 5 mM chloracetamide (Sigma-Aldrich, #C0267)) over night at room temperature in the dark. Peptides were acidified to pH < 2 with tri-fluoracetic acid and desalted on home-made StageTips containing Empore C_{18} disks (Rappsilber et al., 2007). C18 stage tips were activated with 100 μL methanol, 100 μL buffer B (0.1% formic acid, 80% acetonitrile) and twice with 100 μL buffer A (0.1% formic acid). The acidified peptides were added onto the stage tips and washed with 100 μL buffer A. Peptides were eluted with 40–60 μL buffer B and dried-down in a speed vac and resolubilized in 9 μL buffer A (0.1% formic acid in MS grade water) and 1 μL buffer A* (2% acetonitrile, 0.1% tri-flouracetic acid in MS grade water). Peptides were separated using an Easy-nLC 1200 system (Thermo Scientific) coupled to a Q Exactive HF mass spectrometer via a Nanospray-Flex ion source. The analytical column (50 cm, 75 μm inner diameter (NewObjective) packed in-house with C18 resin ReproSilPur 120, 1.9 μm diameter Dr. Maisch) was operated at a constant flow rate of 250 nL/min. Gradients of 90 min were used to elute peptides (Solvent A: aqueous 0.1% formic acid; Solvent B: 80% acetonitrile, 0.1% formic acid). MS spectra with a mass range of 300–1.650 m/z were acquired in profile mode using a resolution of 60.000 [maximum fill time of 20 ms or a maximum of 3e6 ions (automatic gain control, AGC)]. Fragmentation was triggered for the top 15 peaks with charge 2–8 on the MS scan (data-dependent acquisition) with a 30 s dynamic exclusion window (normalized collision energy was 28). Precursors were isolated with a 1.4 m/z window and MS/MS spectra were acquired in profile mode with a resolution of 15,000 (maximum fill time of 80 ms, AGC target of 2e4 ions).

To identify mitochondrial aggregates, the expression of the mtCPY* was induced for 4 h via 0.5% of galactose in raffinose media. Mitochondria were isolated and lysed by the addition of 0.1% Triton X-100 buffer (0.1% Triton X-100; 150 mM NaCl, 5 mM EDTA pH8, 10 mM Tris pH 7.4, 1 mM PMSF, 1x complete protease inhibitor cocktail). Aggregated/pellets (P) and soluble (S) fractions were obtained by centrifugation at 30.000*g*, 4°C for 15 min. The soluble fraction was transferred to a new tube and precipitated by TCA. Afterward S and P were resolubilized in 10μL of SDS containing lysis buffer (50 mM Tris pH 7.5, 2% SDS, 1x complete protease inhibitor cocktail). For Total samples (T) equal amounts of protein were collected in SH buffer and directly resolubilized in 10 μL of SDS lysis buffer. For the Booster and Normalization Channel a total of 200μg protein was used. For the Booster channel protein of all strains from replicate 1 were pooled; the Normalization channel only mitochondrial protein from WT ev ev was used. A sample (calculated with a probable concentration of around 10 μg) of each lysate was subjected to an in-solution tryptic digest using a modified version of the Single-Pot Solid-Phase-enhanced Sample Preparation (SP3) protocol. Here, lysates were added to Sera-Mag Beads (Thermo Scientific, no. 4515-2105-050250, 6515-2105-050250) in 15% formic acid (4 μL) and ethanol (15 μL). The binding of proteins was achieved by shaking for 15 min at room temperature. SDS was removed via 4 subsequent washes with 100 μL of 80% ethanol. Proteins were digested with 0.4 μg of sequencing-grade modified trypsin (Promega, no. V5111) in 2 μL 1 M HEPES in the presence of 1.25 mM Tris(2-carboxyethyl)phosphine(TCEP) and 5 mM chloroacetamide (Sigma-Aldrich, no. C0267) overnight at 25°C. Booster and Normalization samples were digested with the same buffer containing 4 μg of Trypsin. Beads were separated, washed with 10 μL of an aqueous solution of 2% dimethylsulfoxide, and the combined eluates were dried down. In total, four biological replicates were prepared (n = 4). Peptides were reconstituted in 10 μL of H_2O. To each sample 4 μL of TMT10plex (Thermo Scientific, no. 90111) label reagent was added and carried out for 1 h at room temperature. 1 TMT10plex was resolved in 51 μL of acetonitrile (ACN). Excess TMT reagent was quenched by the addition of 4 μL of an aqueous solution of 5% hydroxylamine (Sigma, no. 438227). Mixing ratios were adjusted from the intensities measured in the first run to get equal amounts of peptides. It was aimed for a 2 M excess of the Booster channel to all other samples in T and S and a 5-fold excess in P. Samples of each TMT channel were pooled peptides were acidified with TFA to pH < 2. Desalting/Reversed-Phase cleanup of labeled peptides with 3xC18 stage tips. Followed by pH fractionation (1: pH 4.5, 2: pH 5.2, 3: pH 12.0) with 3xSCX stage tips. Desalting/Reversed-Phase cleanup of labeled peptides with 3xC18

stage tips. For TMT-labelled samples, MS spectra were acquired in profile mode with a mass range of 300–1.650 m/z and a resolution of 120.000 [maximum fill time of 80 ms or a maximum of 3e6 ions (automatic gain control, AGC)]. Fragmentation was triggered for the top 15 peaks with charge 2–8 on the MS scan (data-dependent acquisition) with a 30 s dynamic exclusion window (normalized collision energy was 32). Precursors were isolated with a 0.7 m/z window and MS/MS spectra were acquired in profile mode with a resolution of 60,000 (maximum fill time of 100 ms, AGC target of 1e5 ions). Fixed first mass was set to 100 m/z.

For the quantitative comparison of proteomes of rho^0 and WT cells expressing MTS-Var1 10 OD_{600} of cells were harvested by centrifugation (12,000 g, 5 min) and snap-frozen in liquid nitrogen and stored at −80°C. Cells lysates were prepared in lysis buffer (6 M GdmCl, 10 mM TCEP, 40 mM CAA, 100 mM Tris pH 8.5) using a FastPrep-24 5G homogenizer (MP Biomedicals, Heidelberg, Germany) with 3 cycles of 30 s, speed 8.0 m/s, 120 s breaks, glass beads). Lysates were boiled for 5 min at 96°C and centrifuged (16,000 g, 2 min, 4°C). Protein concentrations were determined using the Pierce BCA Protein Assay (Thermo Scientific, #23225). For protein digestion 25 μg of protein were diluted 1:10 with digestion buffer (10% ACN, 25 mM Tris pH 8.5), next Trypsin and LysC were added in a 1:50 ratio and the reaction was incubated overnight at 37°C. The next day fresh Trypsin was added in a 1:100 ratio for 30 min at 37°C. pH of samples was adjusted to pH < 2 with tri-fluoracetic acid. Desalting/reversed-Phase cleanup with 3x SDB-RPS StageTips. Samples were dried down in speed-vac and resolubilized in 12 μL buffer A^{++} (0.1% formic acid, 0.01% tri-flouracetic acid in MS grade water). Peptides were separated using an Easy-nLC 1200 system (Thermo Scientific) coupled to a Q Exactive HF mass spectrometer via a Nanospray-Flex ion source. The analytical column (50 cm, 75 μm inner diameter (NewObjective) packed in-house with C18 resin ReproSilPur 120, 1.9 μm diameter Dr. Maisch) was operated at a constant flow rate of 250 nL/min. Gradients of 180 min were used to elute peptides (Solvent A: aqueous 0.1% formic acid; Solvent B: 80% acetonitrile, 0.1% formic acid). MS spectra with a mass range of 300–1.650 m/z were acquired in profile mode using a resolution of 60.000 [maximum fill time of 20 ms or a maximum of 3e6 ions (automatic gain control, AGC)]. Fragmentation was triggered for the top 15 peaks with charge 2–8 on the MS scan (data-dependent acquisition) with a 30 s dynamic exclusion window (normalized collision energy was 28). Precursors were isolated with a 1.4 m/z window and MS/MS spectra were acquired in profile mode with a resolution of 15,000 (maximum fill time of 80 ms, AGC target of 2e4 ions).

Analysis of mass spectrometry data

Peptide and protein identification and quantification was done using the MaxQuant software (version 2.0.1.0) (Cox and Mann, 2008, Cox et al., 2011, Tyanova et al., 2016) and a *Saccharomyces cerevisiae* proteome database obtained from Uniprot. Protein N-terminal acetylation and Met oxidation were specified as variable modifications and Cys carbamidomethylation as fixed modification. The ''Requantify'' and ''Second Peptides'' options were deactivated. False discovery rate was set at 1% for peptides, proteins and sites, minimal peptide length was 7 amino acids. For label-free data, the LFQ normalization algorithm and second peptides was enabled. Match between run was applied within each group of replicates. False discovery rate was set at 1% for peptides, proteins and sites, minimal peptide length was 7 amino acids.

The protein groups identified in each mass spectrometry data set were processed and analyzed in parallel using R programming language (version 4.2.1). (R Core Team (2018). R: A language and environment for statistical computing. R Foundation for Statistical Computing, Vienna, Austria). For all datasets, the MaxQuant output was first filtered to remove contaminants, reverse hits and proteins identified by site only.

The LFQ datasets were further filtered excluding proteins that were identified in less than three replicates (N = 4) of every condition. This resulted in 472 (Var1- & Atp1-GFP pulldowns), 590 (Pim1-GFP pulldowns), 2093 (Hsp78-GFP pulldowns) and 4103 (whole-cell extracts) robustly identified protein groups whose label-free quantification (LFQ) intensities were log2-transformed subsequently. Lastly, missing values were imputed by sampling N = 4 values from a normal distribution (seed = 12345) and using them whenever there are no valid values in a quadruplicate of a condition. Different for each dataset, the mean of this normal distribution corresponds to the 1% percentile of LFQ intensities, and its standard deviation is determined as the median of LFQ intensity sample standard deviations calculated within and then averaged over each quadruplicate.

For the TMT dataset, processing was performed on the log2-transformed reporter ion intensities for each protein fraction's 10plex (total, soluble and pellet) separately. To allow for the normalization of intensities from the different fractions, only proteins with at least one valid value in the normalization channel of the 10plex were considered. Furthermore, only proteins with at least 2 values in at least 2 conditions were included. After removing all non-mitochondrial proteins as indicated by Morgenstern et al. (https://doi.org/10.1016/j.celrep.2017.06.014), this resulted in 677 robustly identified, mitochondrial proteins in the overlap between all fractions. Next, the effects of the replicate batch on the protein intensities were removed using the function removeBatchEffect implemented in the limma R-package (version 3.52.4)(Ritchie et al., 2015). To normalize intensities between the 10plexes of the three fractions, the intensities from the normalization channel were averaged for each protein and subtracted from the values in the corresponding conditions within each 10plex. Finally, soluble and pellet ratios (S/T and P/T) were calculated by subtracting the average intensity of the total fraction from the soluble and pellet fraction values respectively for each protein and condition.

Principal component analysis was carried out for each dataset using the package *pcaMethods* (Stacklies et al., 2007) on the processed and standardized LFQ intensities of those protein groups with an ANOVA F-statistic p value <0.05 between all replicate groups to filter for proteins with a discernable degree of variance between conditions.

Protein groups were statistically analyzed using pairwise, two-sided Welch's t-tests on the processed LFQ intensities between the replicates of respective control and treatment conditions. Only proteins with valid values in the treatment conditions were considered

for comparison. Log2 fold changes were derived as the tested difference of means and the resulting p values were adjusted for multiple testing using the Benjamini-Hochberg procedure (Benjamini and Hochberg, 1995). All relevant test results are listed in Table S1.

Fluorescence microscopy

For microscopy cells were grown to mid-log phase and treated with 2 mg/mL chloramphenicol or 7.5 mg/mL cycloheximide for 2 h before shifting cells to the indicated heat stress conditions. To express proteins under the GAL1 promotor 0.5% Gal was added to the medium. To stop expression cells were harvested (5 min 5000 g) and washed twice with H_2O before resuspension in liquid media. 1 OD was harvested via centrifugation and cell pellets were resuspended in 30 μL of H_2O. 3 μL were pipetted onto a glass slide and covered with a coverslip. Manual microscopy was performed using a Leica Dmi8 Thunder Imager. Images were acquired using an HC PL APO100x/1,44 Oil UV objective with Immersion Oil Type A 518 F. For excitation of GFP 475 nm mNeonGreen 510 nm, mScarletI and mCherry 575 nm was used. All images were taken as Z-stacks. Image analysis was done with the LAS X software and further processing of images was performed in Fiji/ImageJ.

Colocalization of mtCPY*-mScarlet and Hsp78-GFP was quantified using FiJi and the Colocalization Analysis2 Plugin (Colog2) and represented as the Pearson's correlation coefficient (PCC).

QUANTIFICATION AND STATISTICAL ANALYSIS

Unless otherwise indicated, experiments were performed in n = 3 independent biological replicates and the mean values and the standard deviations are present in the figures. p values are indicated in the respective plots and were assessed using standard statistical tests as described in the respective figure legend and descriptions in the STAR Methods section.